Immunity

CellPress

Article

An Oncogenic Alteration Creates a Microenvironment that Promotes Tumor Progression by Conferring a Metabolic Advantage to Regulatory T Cells

Shogo Kumagai,[1,2] Yosuke Togashi,[1,*] Chika Sakai,[1] Akihito Kawazoe,[3] Masahito Kawazu,[4] Toshihide Ueno,[4] Eiichi Sato,[5] Takeshi Kuwata,[6] Takahiro Kinoshita,[7] Masami Yamamoto,[8] Sachiyo Nomura,[9] Tetsuya Tsukamoto,[10] Hiroyuki Mano,[4] Kohei Shitara,[3] and Hiroyoshi Nishikawa[1,2,11,*]

[1]Division of Cancer Immunology, Research Institute/Exploratory Oncology Research and Clinical Trial Center (EPOC), National Cancer Center, Tokyo/Chiba, Japan
[2]Department of Immunology, Nagoya University Graduate School of Medicine, Nagoya, Japan
[3]Department of Gastrointestinal Oncology, National Cancer Center Hospital East, Chiba, Japan
[4]Division of Cellular Signaling, Group for Cancer Development and Progression, National Cancer Center Research Institute, Tokyo, Japan
[5]Department of Pathology, Institute of Medical Science, Tokyo Medical University, Tokyo, Japan
[6]Department of Pathology and Clinical Laboratories, National Cancer Center Hospital East, Chiba, Japan
[7]Department of Gastric Surgery, National Cancer Center Hospital East, Chiba, Japan
[8]Division of Physiological Pathology, Department of Applied Science, School of Veterinary Nursing and Technology, Nippon Veterinary and Life Science University, Tokyo, Japan
[9]Department of Gastrointestinal Surgery, Graduate School of Medicine, The University of Tokyo, Tokyo, Japan
[10]Department of Pathology, Graduate School of Medicine, Fujita Health University, Aichi, Japan
[11]Lead Contact
*Correspondence: ytogashi1584@gmail.com (Y.T.), hnishika@ncc.go.jp (H.N.)
https://doi.org/10.1016/j.immuni.2020.06.016

SUMMARY

Only a small percentage of patients afflicted with gastric cancer (GC) respond to immune checkpoint blockade (ICB). To study the mechanisms underlying this resistance, we examined the immune landscape of GC. A subset of these tumors was characterized by high frequencies of regulatory T (Treg) cells and low numbers of effector T cells. Genomic analyses revealed that these tumors bore mutations in *RHOA* that are known to drive tumor progression. *RHOA* mutations in cancer cells activated the PI3K-AKT-mTOR signaling pathway, increasing production of free fatty acids that are more effectively consumed by Treg cells than effector T cells. *RHOA* mutant tumors were resistant to PD-1 blockade but responded to combination of PD-1 blockade with inhibitors of the PI3K pathway or therapies targeting Treg cells. We propose that the metabolic advantage conferred by *RHOA* mutations enables Treg cell accumulation within GC tumors, generating an immunosuppressive TME that underlies resistance to ICB.

INTRODUCTION

Immune checkpoint blockade (ICB) therapies improve the survival of patients with multiple types of cancer, including malignant melanoma, lung cancer, and gastric cancer (GC) (Borghaei et al., 2015; Kang et al., 2017; Reck et al., 2016; Robert et al., 2015; Schachter et al., 2017; Weber et al., 2015). Various immunological facets, including PD-ligand 1 (PD-L1) expression in tumor tissues and mutation burden in tumor cells, are reportedly associated with clinical responses of ICB (Borghaei et al., 2015; Kang et al., 2017; Reck et al., 2016; Rizvi et al., 2015; Robert et al., 2015; Schachter et al., 2017; Weber et al., 2015). The ratio of CD8^{+} T cells to regulatory T (Treg) cells in the tumor microenvironment (TME) is also an important factor for prognosis and clinical efficacies (Ayers et al., 2017; Curiel et al., 2004; Sato et al., 2005). In cancer settings, various chemokines that are pro-

duced by tumor-infiltrating immune cells have been reported to contribute the migration of immune cells including both effector T cells and suppressive cells into the TME (Fridman et al., 2012; Nagarsheth et al., 2017; Togashi et al., 2019). As Treg cell migration is also dominantly triggered by chemokine networks in the TME, Treg cells are often detected with effector T cells in the inflamed TME (Nagarsheth et al., 2017; Spranger et al., 2013; Togashi et al., 2019). However, some tumors with the noninflamed TME contain abundant Treg cells, suggesting multiple mechanisms of Treg cell expansion in the TME, other than chemokine networks.

As cancer cells mainly consume glucose to fuel aerobic glycolysis for their survival (the Warburg effect), low-glucose and hypoxic conditions that are unfavorable for T cell survival and functions develop in the TME (Gatenby and Gillies, 2004; Ho and Kaech, 2017; Warburg, 1956). The low-glucose conditions
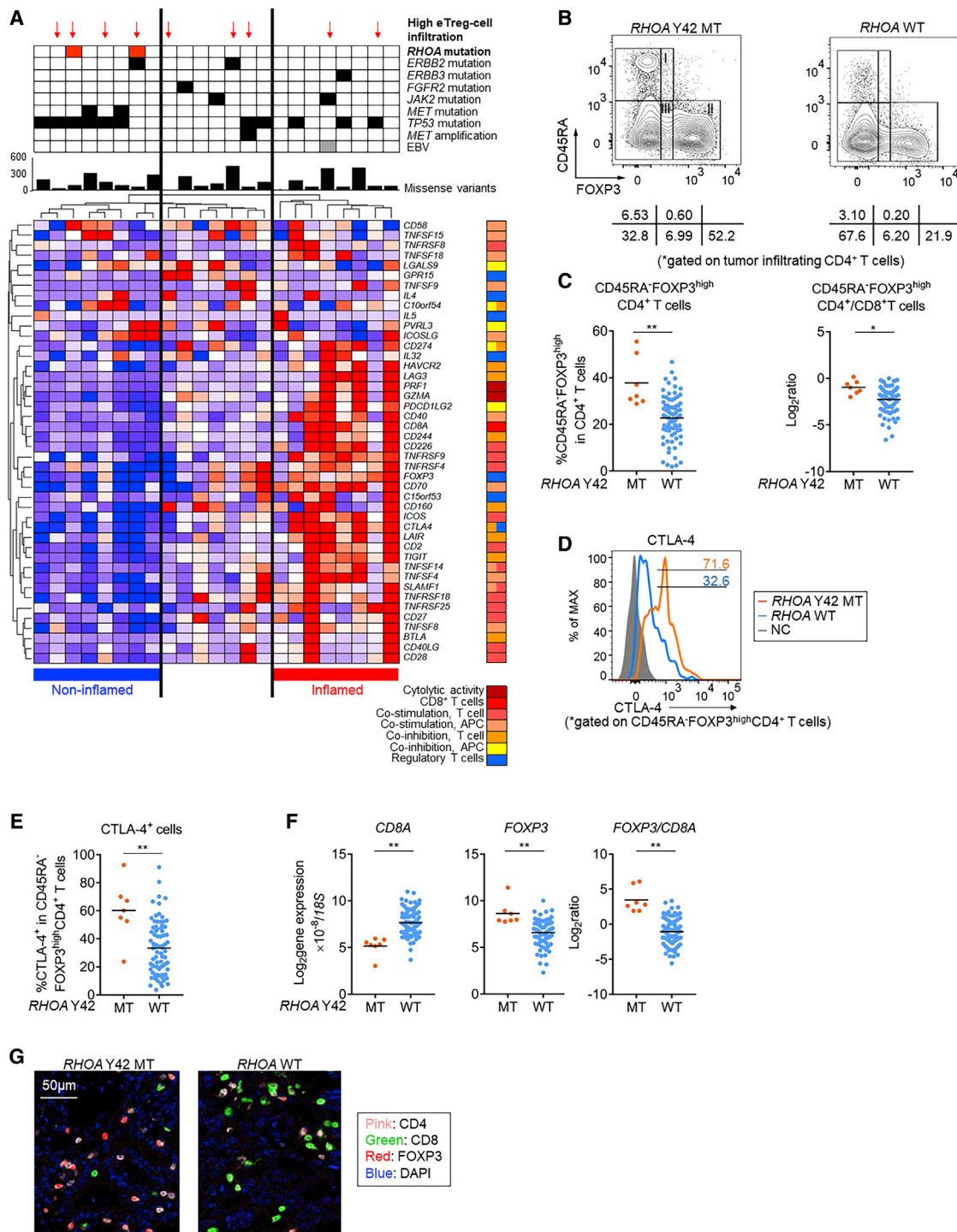
Figure 1. *RHOA* Y42-Mutated GCs Harbor High eTreg Cell Infiltration Regardless of the Noninflamed Status of the TME

(A) RNA from twenty-three GC samples was subjected to RNA-seq and clustered by immune-related gene sets (CD4+ Treg cells, CD8+ T cell, co-stimulation APC and T cell, co-inhibition APC and T cell, and cytolytic activity). WES was performed with the same tumors. Representative driver gene alterations (filled sections) and the number of missense variants (bars) are shown. Red arrows indicate samples where the tumor-infiltrating eTreg cell proportion in the CD4+ T cell population is >20%. Red, *RHOA* Y42C; black, other representative driver gene alterations; and gray, EBV.

(B and C) Representative contour plots of eTreg cells in 85 advanced GC samples classified according to *RHOA* gene status (B) and summaries (C) are shown. TILs from tumor tissue samples were subjected to FCM. I, fraction I (naive Treg cells); II, fraction II (eTreg cells); III, fraction III (non-Treg cells).

(D and E) Representative histogram plots of CTLA-4 expression by eTreg cells in advanced GC samples classified according to *RHOA* gene status (D) and summary (E) are shown. TILs from tumor tissue samples were subjected to FCM.

(legend continued on next page)

Immunity
Article

CellPress

in the TME reportedly contribute to resistance to cancer immunotherapy, via inhibiting the resurgence of effector T cells (Chang et al., 2015). However, how Treg cells remain abundant and strongly immunosuppressive in the TME, given the unfavorable conditions for T cell proliferation and maintenance, is not clear. One plausible explanation is that effector T cells and Treg cells harbor different metabolic profiles for their survival and function (Wang et al., 2017). Indeed, Treg cells require mitochondrial metabolism to maintain immunosuppressive function (Weinberg et al., 2019).

The response rate to PD-1 blockade is much lower in patients afflicted with GC than patients afflicted with malignant melanoma or lung cancer (Borghaei et al., 2015; Kang et al., 2017; Reck et al., 2016; Robert et al., 2015; Schachter et al., 2017; Shitara et al., 2018; Weber et al., 2015). We therefore considered that GC may establish an immunosuppressive TME. Thus, we aimed at elucidating the immunological landscape in the TME of GC. We found that some GC tissue samples exhibited an immunosuppressive TME that was characterized by abundant Treg cells in spite of the noninflamed TME. These tumors harbored Y42 mutations in *RHOA*, well-known driver mutations in GC (Cancer Genome Atlas Research Network., 2014; Kakiuchi et al., 2014; Wang et al., 2014). We found that the increased production of free fatty acids (FFAs) by *RHOA* Y42-mutated GC cells, mediated via the PI3K pathway, supported Treg cell accumulation in the low-glucose TME. The combination of PD-1 blockade and PI3K blockade overcame resistance of *RHOA* Y42-mutated tumors to PD-1 blockade in mouse models. Our findings provide insight into the mechanisms whereby tumors promote the accumulation of immune-suppressive cells and suggest a combination therapy approach that may benefit GC patients.

RESULTS

Patients with *RHOA* Y42 Mutations Have an Immunosuppressive TME Characterized by Treg Cell Accumulation

We first analyzed the immunological status (inflamed or noninflamed) and cell types in tumor samples from 23 GC patients who had undergone surgical resection (Table S1). According to immune-related gene expression evaluated by RNA sequencing (RNA-seq), eight tumor samples had a noninflamed TME, and the remaining eight tumor samples had an inflamed TME (Figure 1A). In addition to RNA-seq, whole-exome sequencing (WES) was performed with the same samples and showed no correlation between the immunological status of the tumors (inflamed or noninflamed) and tumor mutational burden (TMB), which is reportedly important for antitumor immunity (Rizvi et al., 2015; Rooney et al., 2015) (Figure 1A).

To precisely evaluate Treg cells in the TME, given the transient upregulation of FOXP3 expression upon T cell receptor (TCR) stimulation in naive T cells (Tran et al., 2007), tumor-infiltrating lymphocytes (TILs) were subjected to flow cytometry (FCM) and assessed with our classification dividing human

FOXP3$^+$CD4$^+$ cells into three subpopulations based on the expression levels of the naive cell marker CD45RA and FOXP3 (Miyara et al., 2009; Saito et al., 2016; Togashi et al., 2019): naive Treg cells [Fraction (Fr.) I: nTreg cells, CD45RA$^+$FOXP3^{low}CD4$^+$] with weak immunosuppressive function, effector Treg cells (Fr. II: eTreg cells, CD45RA$^-$FOXP3^{high}CD4$^+$) with strong immunosuppressive function, and non-Treg cells (Fr. III: CD45RA$^-$FOXP3^{low}CD4$^+$) without immunosuppressive function (Figures S1A and S1B). From the FCM and RNA-seq data, four patients bore an immunosuppressive TME that was characterized by Treg cell accumulation regardless of the noninflamed status of the TME (Figure 1A), although Treg cells are generally accompanied by effector T cell infiltration in the inflamed TME (Spranger et al., 2013). The WES analysis revealed that two of these patients possessed the *RHOA* Y42C mutation. Accordingly, GC patients with *RHOA* Y42C (*RHOA* Y42C-GCs) harboring a low TMB exhibited lower expression of immune-related genes, including *CD8A*, *IFNG*, and *CD274*, than GC patients lacking the mutation (Figures S1C and S1D). The frequency of tumor-infiltrating eTreg cells, the ratio of tumor-infiltrating eTreg cells/CD8$^+$ T cells, and the expression of CTLA-4, a key molecule in Treg cell-mediated immunosuppression (Wing et al., 2008), by tumor-infiltrating eTreg cells tended to be higher in *RHOA* Y42C-GCs than in *RHOA* wild-type (WT) GCs (Figures S1A, S1B, S1E and S1F). To validate the immunosuppressive TME of GCs with the *RHOA* Y42 mutations, 85 advanced GC patients' samples from another cohort were analyzed (Table S2). *RHOA* Y42C or Y42S mutation was detected in 7 (5 or 2, respectively) GC samples with digital polymerase chain reaction (PCR). The frequency of eTreg cells, the ratio of eTreg cells/CD8$^+$ T cells, and the expression of CTLA-4 by eTreg cells in the TME were higher in *RHOA* Y42-mutated GCs than in *RHOA* WT GCs (Figures 1B–1E). Lower expression of *CD8A* and higher expression of *FOXP3* in *RHOA* Y42-mutated GCs than *RHOA* WT GCs were detected with real-time qRT-PCR (Figure 1F). Higher eTreg cell infiltration was also observed with immunohistochemistry (IHC) (Figures 1G and S1G). The analysis of the Cancer Genome Atlas (TCGA) data confirmed higher expression of *FOXP3* and higher ratio of *FOXP3/CD8A* expression in *RHOA* Y42-mutated GCs compared with *RHOA* WT-GCs (Cancer Genome Atlas Research Network., 2014) (Figure S1H). These findings suggest that activated eTreg cells accumulate in the TME in spite of the noninflamed phenotype in *RHOA* Y42-mutated GCs.

RHOA Y42 Mutations Increase the Activity of the PI3K-AKT Signaling Pathway and Reduces Production of Chemokines Associated with Effector T Cell Recruitment

To explore how the noninflamed TME was developed by *RHOA* Y42 mutations, comprehensive gene expression was examined with microarray analyses using *RHOA* WT or Y42C-overexpressing human GC cell lines (MKN1^{WT}, MKN1^{Y42C}, MKN45^{WT}, and MKN45^{Y42C}) and murine gastrointestinal cell lines (MC-38^{WT},

---

(F) *CD8A* and *FOXP3* expression (left and middle) and the ratio of *FOXP3* to *CD8A* expression (right) in advanced GC samples according to *RHOA* gene status was examined by real-time qRT-PCR.

(G) Representative pictures of multiplexed IHC for CD4 (pink), CD8 (green), FOXP3 (red), and DAPI (blue). *p < 0.05; **p < 0.01; MT, mutation; WT, wild-type; and NC, negative control.
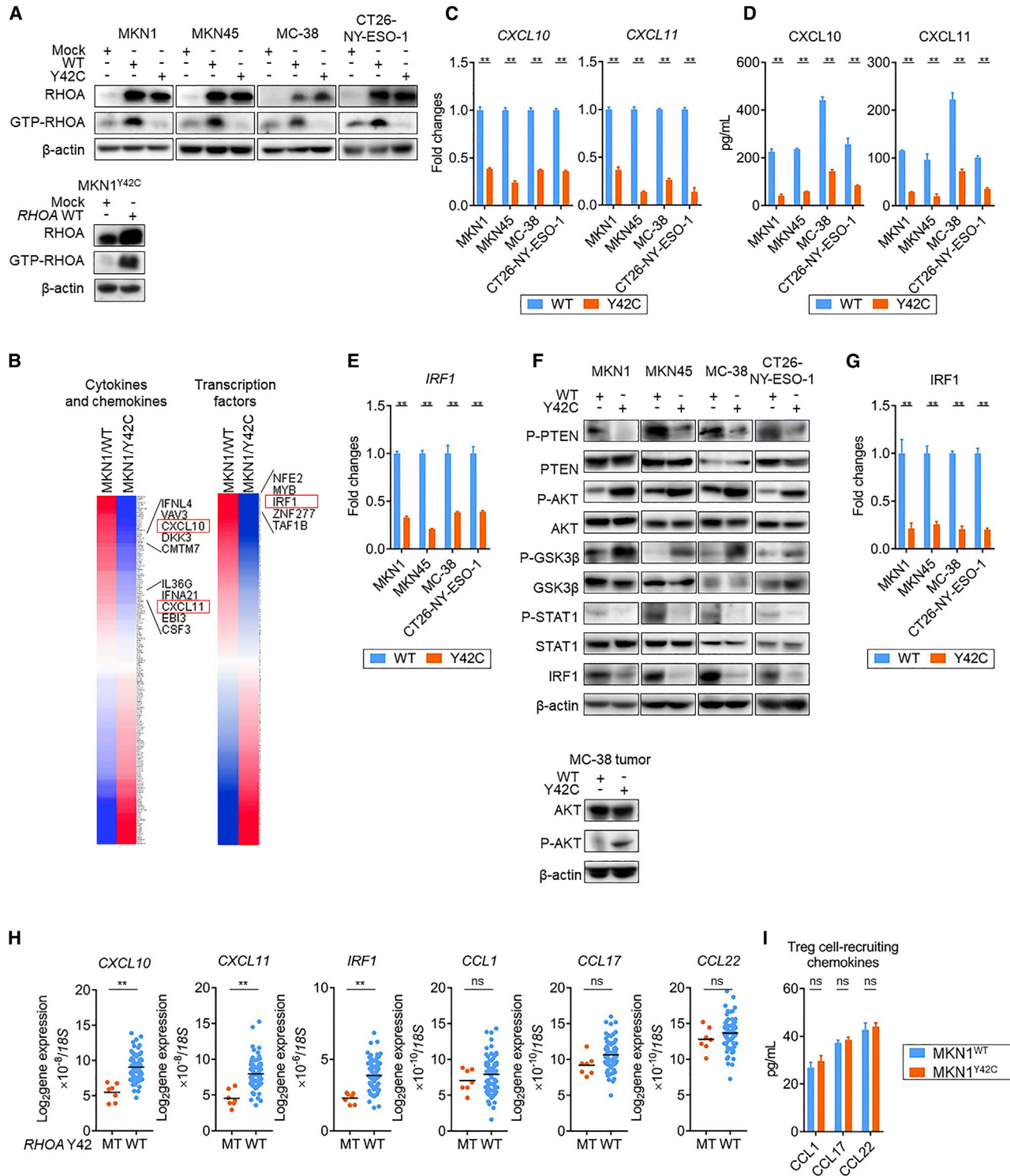
Figure 2. *RHOA* Y42 Mutations Reduce CXCL10, CXCL11, and IRF1 Expression via the Activation of PI3K-AKT Signaling Pathways

(A) *RHOA* WT or *RHOA* Y42C was retrovirally transduced into two human GC cell lines (MKN1 and MKN45) and two murine gastrointestinal cell lines (MC-38 and CT26-NY-ESO-1) (top). *RHOA* WT was retrovirally transduced into MKN1^{Y42C} (bottom). Representative blots of Rhotekin pull-down assays from three independent experiments are shown.

(B) MKN1^{WT} and MKN1^{Y42C} cells were subjected to microarray analysis. The expression of cytokines and chemokines (left) or transcriptional factors (right) based on gene ontology (GO) terms was compared.

Immunity
Article

CellPress

MC-38^{Y42C}, CT26-NY-ESO-1^{WT}, and CT26-NY-ESO-1^{Y42C}) (Figure 2A). When we focused on cytokine or chemokine gene expression, the expression of *CXCL10* and *CXCL11*, which recruit effector CD8$^+$ T cells (Gorbachev et al., 2007; Griffith et al., 2014; Hensbergen et al., 2005; Van Raemdonck et al., 2015; Zumwalt et al., 2015), was lower in MKN1^{Y42C} cells than in MKN1^{WT} cells (Figure 2B). In addition, differential analyses of transcription factor expression between MKN1^{WT} and MKN1^{Y42C} cells uncovered the concurrent reduction in the expression of *IRF1*, which reportedly regulates *CXCL10* and *CXCL11* (Harikumar et al., 2014; Yang et al., 2007) (Figure 2B). Real-time qRT-PCR, enzyme-linked immunosorbent assay (ELISA), and western blotting analyses confirmed the simultaneous reduction in IRF1 expression and CXCL10 and CXCL11 expression in the *RHOA* Y42C GC cell lines (Figures 2C–2G). Furthermore, similar trends were observed in gene expression of clinical GC samples (Figures 2H and S1I). Overall, the *RHOA* Y42 mutations decrease the levels of effector T cell-recruiting chemokines such as CXCL10 and CXCL11 via the reduction of IRF1 expression.

Gene alterations in the effector domain of *RHOA,* including Y42C, impair binding to effector proteins, thereby decaying the signaling pathways of RHOA (Bae et al., 1998; Sahai et al., 1998; Wang et al., 2014). Accordingly, *RHOA* Y42C cells markedly reduced the amount of the GTP-associated form detected by Rhotekin-Rho binding domain pull-down assays, which was recovered by expression of *RHOA* WT (Figure 2A). This reduction decreased phosphorylation of PTEN and increased phosphorylation of AKT, suggesting a defect in the RHOA/ROCK/PTEN signaling pathways (Figure 2F). Phosphorylated GSK3β, which is induced by the PI3K-AKT signaling pathways, reportedly suppresses STAT1 (Tsai et al., 2009), a well-known transcription factor of IRF1 (Ramana et al., 2000). In line with this, the increased phosphorylated GSK3β level induced by *RHOA* Y42C led to the suppression of STAT1, resulting in IRF1 expression reduction (Figures 2F and 2G). Therefore, *RHOA* Y42C reduces the expression of *CXCL10* and *CXCL11* by upregulating the PI3K-AKT signaling pathways (Figure S2A).

RHOA Y42-MutatedGCs with High eTreg Cell Infiltration in the TME Efficiently Produce FFAs via PI3K-AKT-mTOR Pathway

The protein expression of CCL1, CCL17, and CCL22, which reportedly recruit eTreg cells (Curiel et al., 2004; Hoelzinger et al., 2010; Mantovani et al., 2017; Togashi et al., 2019), by MKN1^{Y42C} and MKN1^{WT} cells showed a comparable expression regardless of *RHOA* gene status (Figure 2I). Rather, a trend in lower expression of *CCL1*, *CCL17,* and *CCL22* in *RHOA* Y42-mutated GCs compared with *RHOA* WT GCs was observed (Figure 2H and S1I), suggesting that other mechanism(s) may be mainly involved in eTreg cell accumulation and immunosuppression in the TME of *RHOA* Y42-mutated GCs.

To elucidate the mechanism(s) of eTreg cell accumulation and immunosuppression by *RHOA* Y42 mutations, we employed Gene Set Enrichment Analysis (GSEA) of the RNA-seq, which revealed that the gene set related to fatty acid metabolism was enriched in *RHOA* Y42C GCs (Figure 3A). Consistently, the expression of *FASN* (encoding FAS), which plays an important role in fatty acid synthesis (Wakil, 1989), was higher in *RHOA* Y42-mutated GCs than in *RHOA* WT GCs (Figure 3B and S1I). eTreg cells possess a different metabolic profile compared with effector T cells that preferentially utilize glucose: Treg cells depend on lipid oxidation for their survival (Michalek et al., 2011). Cancer cells deprive glucose from the TME and produce fatty acids through *de novo* synthesis from glucose (the Warburg effect) (Currie et al., 2013; Röhrig and Schulze, 2016), resulting in lower glucose concentration in the TME than in the periphery (Figure S3A). Tumor-infiltrating Treg cells take up more FFAs than other T cell subsets (Muroski et al., 2017). Therefore, we hypothesized that *RHOA* Y42-mutated GCs produced larger amounts of FFAs via increased FAS expression, which contributed to the prolonged survival of eTreg cell subset in the TME compared with that of other effector T cell subsets. In line with this hypothesis, both *FASN* mRNA and FAS protein expression was higher in *RHOA* Y42C cell lines than in *RHOA* WT cell lines (Figures 3C–3E). The activation of PI3K-AKT/mTOR/S6K signaling pathways elevates FAS expression via transcription factor SREBP-1 (Düvel et al., 2010; Peterson et al., 2011; Porstmann et al., 2008). We then examined these signaling pathways using the cell lines, and the elevations in these signaling pathways in the *RHOA* Y42C-overexpressing cell lines were observed by western blotting (Figure 3D). Accordingly, the total concentration of FFAs in the culture was higher in the *RHOA* Y42C cell line culture than in the *RHOA* WT cell line culture (Figure 3F). In addition, liquid chromatography-mass spectrometry (LC-MS) confirmed the higher concentration of FFA species in the culture of MKN1^{Y42C} cells than in that of MKN1^{WT} cells

(C) *CXCL10* and *CXCL11* expression in *RHOA* WT- or Y42C-expressing cell lines were examined with real-time qRT-PCR. Fold changes relative to the *RHOA* WT cell lines are shown.

(D) The concentrations of CXCL10 and CXCL11 in the culture of *RHOA* WT or Y42C cell lines were analyzed by ELISA. *RHOA* WT and Y42C cell lines were cultured with RPMI medium containing 10% FBS. 48 h later, the concentrations of CXCL10 and CXCL11 were examined.

(E) *IRF1* expression in *RHOA* WT or Y42C cell lines was evaluated with real-time qRT-PCR. Fold changes relative to the *RHOA* WT cell lines are shown.

(F and G) The protein expression of PI3K-AKT signaling pathways in *RHOA* WT or Y42C cell lines was examined by western blotting (F, top). MC-38^{WT} or MC-38^{Y42C} cells (1.0 × 10^6) were injected subcutaneously into C57BL/6 mice on day 0 (N = 3). Protein was extracted from the tumors on day 12. The protein expression of total and phosphorylated AKT in MC-38^{WT} or MC-38^{Y42C} tumors was examined by western blotting. Representative blots of western blotting are shown (F, bottom). Summary of quantified IRF1 (IRF1/β-actin) expression in *RHOA* Y42C cell lines relative to that in *RHOA* WT cell lines from three independent experiments is shown (G). Means from three independent experiments are presented.

(H) Gene expression in advanced GC samples according to *RHOA* gene status was examined by real-time qRT-PCR.

(I) The concentrations of CCL1, CCL17, and CCL22 in the culture medium of MKN1^{WT} or MKN1^{Y42C} were analyzed by ELISA. MKN1^{WT} or MKN1^{Y42C} were cultured with RPMI medium containing 10% FBS. 48 h later, the concentrations of CCL1, CCL17, and CCL22 were examined. β-actin and *18S* ribosomal RNA were used as internal controls for protein and mRNA expression analyses, respectively. Bars, mean; error bars, SEM; **p < 0.01; MT, mutation; WT, wild-type; and ns, not significant.
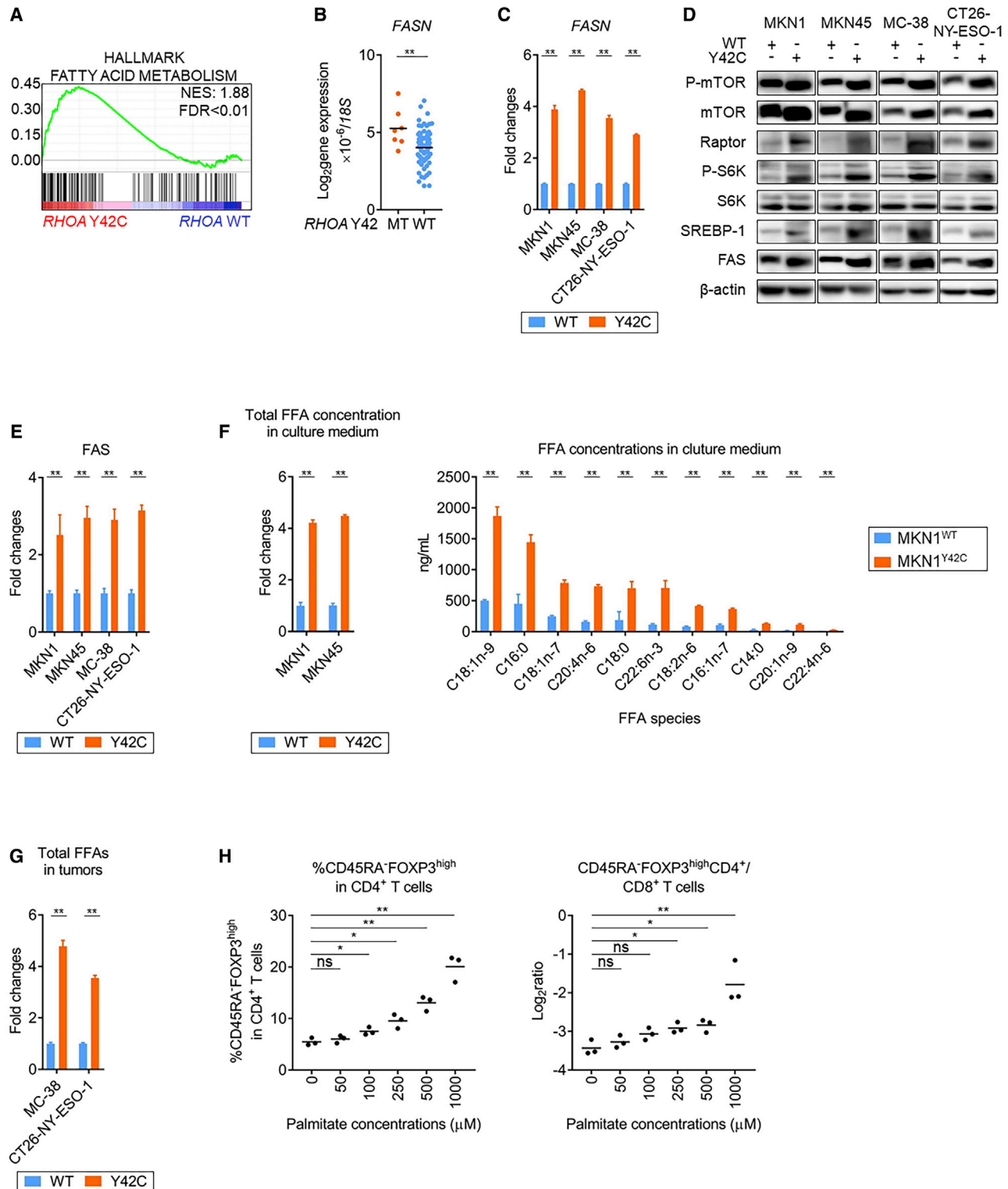
Figure 3. RHOA Y42 Mutations Promote Treg Cell Survival through Increased FFA Production
(A) Fatty acid metabolism-related genes based on GSEA in *RHOA* Y42-mutated GCs were compared with those in *RHOA* WT GCs using RNA-seq data from surgically resected GC samples.
(B) *FASN* expression in advanced GC samples according to *RHOA* gene status was examined by real-time qRT-PCR.
(C) *FASN* expression in *RHOA* WT or Y42C cell lines was analyzed with real-time qRT-PCR. Fold changes relative to the *RHOA* WT cell lines are shown.

(legend continued on next page)

(Figure 3F). Furthermore, we assessed the differences in the total content of FFAs of tumors between *RHOA* WT tumors and *RHOA* Y42C tumors. MC-38^{Y42C} and CT26-NY-ESO-1^{Y42C} tumors also harbored larger amounts of FFAs compared with the corresponding WT cells *in vivo* (Figure 3G). These results indicate that *RHOA* Y42C further increases FFA production via the activation of PI3K-AKT-mTOR-S6K signaling pathways compared with *RHOA* WT (Figure S2B).

Higher FFA Concentration in a Low-Glucose Condition Promotes Treg Cell Accumulation

The higher FFA production by *RHOA* Y42C cancer cells prompted us to explore whether the abundant FFAs in the TME contributed to the prolonged survival of Treg cells. To this end, we employed a low-glucose medium supplemented with increasing concentrations of palmitate to culture peripheral blood mononuclear cells (PBMCs) from healthy individuals. In a concentration-dependent manner, the frequency of eTreg cells increased, resulting in a higher ratio of eTreg cells:CD8$^+$ T cells (Figure 3H). To further confirm the dominant Treg cell expansion compared with other T cell subsets, we sorted CD8$^+$ T cells, CD45RA$^-$CD25$^-$CD4$^+$ T cells (conventional CD4$^+$ T cells; conv CD4$^+$ T cells) and CD45RA$^-$CD25^{high}CD4$^+$ T cells (eTreg cells) from PBMCs and each T cell subset was separately cultured to evaluate the proliferation and apoptosis in the titrated concentrations of FFAs (palmitate or oleate) (Figures S3B–S3H). eTreg cells were more proliferative and less apoptotic compared with other T cell subsets in response to increasing concentration of FFAs under a low-glucose condition, while every T cell subset consumed FFAs under a low-glucose condition (Figures S3B–S3H). In addition, eTreg cells exhibited a stronger suppressive activity in an FFA concentration-dependent manner in a low-glucose condition (Figures S3I and S3J).

We next addressed the differences in fatty acid metabolism among T cell subsets *in vivo* using the murine MC-38 cell line. Lipid uptake and content, which were assessed with BODIPY FL C16 and 493, respectively, were higher in Foxp3$^+$CD4$^+$ cells (Treg cells) than in Foxp3$^-$CD4$^+$ T cells or CD8$^+$ T cells in the TME (Figures 4A and 4B). Additionally, the expression of molecules related to FFA uptake and metabolism, including CD36 (a scavenger receptor mediating the uptake of FFAs), CPT1A (the rate-limiting enzyme in long-chain fatty acid oxidation), PPARα, and PPARγ in Treg cells was higher than that in Foxp3$^-$CD4$^+$ T cells or CD8$^+$ T cells (Figures 4C–4E). In accordance with the animal model data, TILs from GC patients (see Table S3 for patient characteristics) showed higher lipid uptake and content in

eTreg cells than in Foxp3$^-$CD4$^+$ T cells or CD8$^+$ T cells (Figures 4F and 4G). The differences in glucose uptake among T cell subsets in the TME were also examined. Compared with Treg cells, CD8$^+$ T cells exhibited increased glucose uptake (assessed with 2-NBDG) accompanied by higher expression of GLUT1 (Figures 4H and 4I). Overall, Treg cells effectively utilize FFAs for their survival compared with the other T cell subsets in the TME, whereas conventional CD4$^+$ T cells and CD8$^+$ T cells are likely to depend on glucose consumption.

To validate the importance of this metabolic change for Treg cells, we investigated the effects of FFAs on tumor-infiltrating lymphocytes using *Fasn*-expressing MC-38 murine cell line (MC-38^{Fasn}) that produced FFAs (Figures 4J and 4K). The frequency and the number (counts/tumor weight) of Treg cells, and the ratio of Treg cells/CD8$^+$ T cells in the TME were higher in MC-38^{Fasn} tumors than in MC-38^{mock} tumors (Figures 4L–4N). CTLA-4 expression by Treg cells in the TME was higher in the MC-38^{Fasn} tumors than in the MC-38^{mock} tumors (Figures 4O and 4P), suggesting the importance of FFAs for the survival and immunosuppressive function of Treg cells. Additionally, antitumor effects with anti-PD-1 monoclonal antibody (mAb) observed in MC-38^{mock} tumors were dampened in MC-38^{Fasn} tumors (Figure 4Q). Taken together, higher amounts of FFAs in the TME not only contribute to the better survival and immunosuppressive function of Treg cells, but also weaken the antitumor efficacy of anti-PD-1 mAb.

RHOA Y42 Mutations Develop an Immunosuppressive TME *In Vitro* and *In Vivo*

We further explored the critical role of FFAs for the better survival and immunosuppressive function of Treg cells in *RHOA* Y42-mutated tumors. Sorted eTreg cells, conv CD4$^+$ T cells, or CD8$^+$ T cells were cultured with the supernatants from MKN1^{WT} or MKN1^{Y42C} cells to examine the proliferation and apoptosis of each T cell subset (Figures S2C–S2G). eTreg cells were more proliferative and less apoptotic than other T cell subsets, thereby the number of eTreg cells was higher in the cultures with supernatants from MKN1^{Y42C} than in those from MKN1^{WT} (Figures S2C–S2G).

To assess the immunological effect of *RHOA* Y42 mutations on the TME of GCs in addition to MC-38, we established *RHOA* WT or *RHOA* Y42C YTN16 (YTN16^{WT} or YTN16^{Y42C})—a murine gastric adenocarcinoma cell line. The frequency and the number of Treg cells and the ratio of Treg cells:CD8$^+$ T cells were higher in *RHOA* Y42C tumors than in *RHOA* WT

(D and E) The protein expression of mTORC1 signaling pathway components in *RHOA* WT or Y42C cell lines was examined by western blotting (D). Summary of quantified FAS (FAS/β-actin) expression in *RHOA* Y42C cell lines relative to that in *RHOA* WT cell lines from three independent experiments is also shown (E).
(F) FFA concentrations in the culture were evaluated using the Free Fatty Acid Quantification Kit (left) and LC-MS (right). *RHOA* WT or Y42C cell lines were cultured with RPMI medium containing 10% lipids without FBS. 48 h later, the concentrations of FFAs were examined.
(G) MC-38^{WT}, MC-38^{Y42C}, CT26-NY-ESO-1^{WT}, or CT26-NY-ESO-1^{Y42C} cells (1.0 × 10^6) were injected subcutaneously into C57BL/6 mice on day 0 (N = 3 per group). Tumor interstitial fluids were extracted from the *RHOA* WT or Y42C MC-38 and CT26-NY-ESO-1 tumors on day 12. Total FFAs in the interstitial fluids of the *RHOA* WT or Y42C MC-38 and CT26-NY-ESO-1 tumors were evaluated by the Free Fatty Acid Quantification Kit. All *in vivo* experiments were performed at least twice.
(H) The frequency of eTreg cells in low-glucose culture medium with the indicated palmitate concentration was assessed. PBMCs stimulated with anti-CD3 mAb and anti-CD28 mAb were cultured in glucose-free RPMI medium supplemented with 10% lipids without FBS, low-glucose (1 mM), and the indicated concentration of palmitate-BSA. 72 h later, the PBMCs were subjected to FCM. Means from three independent experiments are shown. β-actin and *18S* ribosomal RNA were used as internal controls for protein and mRNA expression analyses, respectively. Bars, mean; error bars, SEM; *p < 0.05; **p < 0.01; MT, mutation; WT, wild-type; and ns, not significant.

CellPress
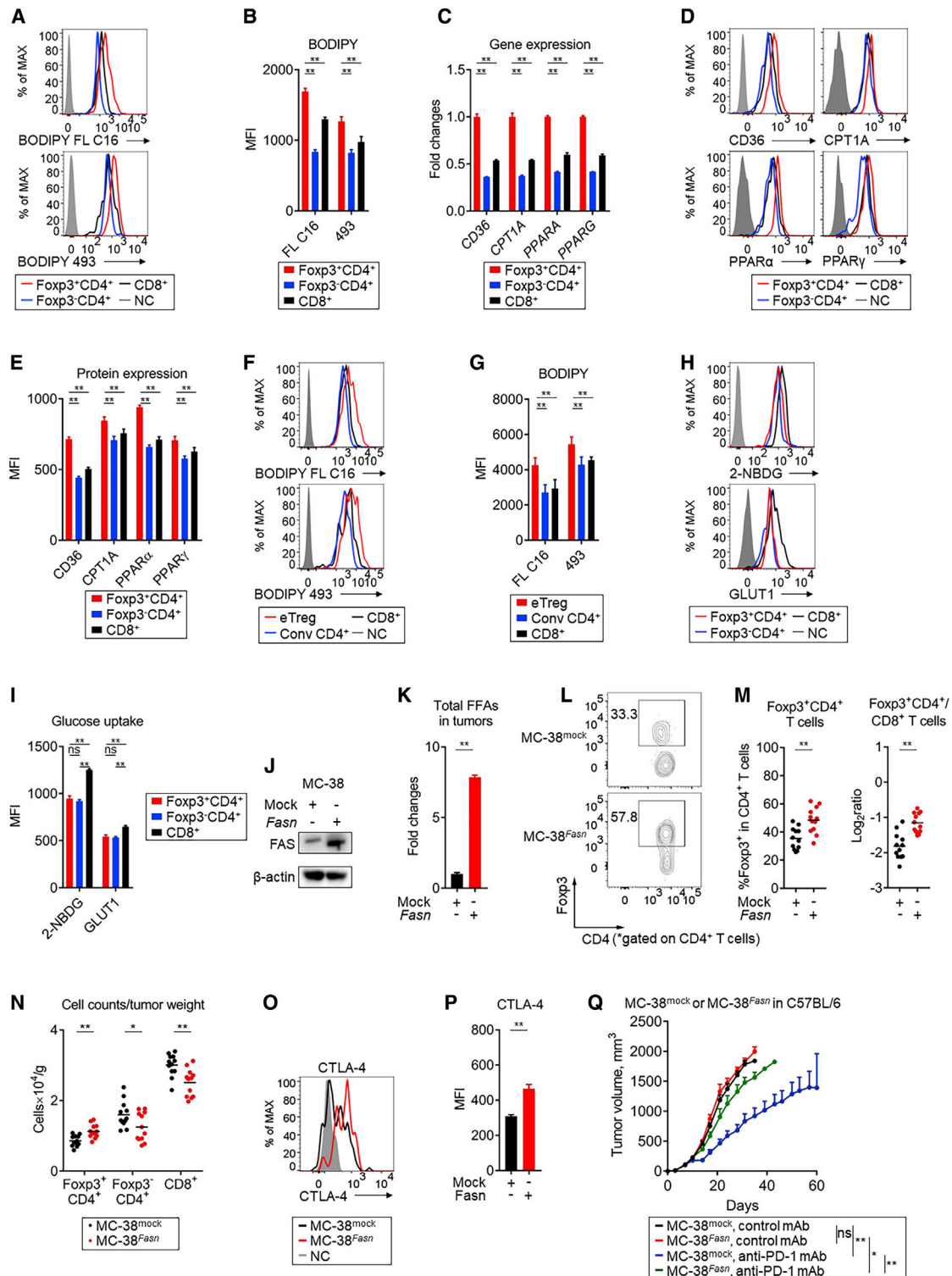
Figure 4. Treg Cells in the TME Take Up and Utilize More FFAs than Other T cell Subsets, and FFA-Producing Tumors Enhance Highly Suppressive Treg Cells and Dampen Anti-Tumor Efficacy of Anti-PD-1 mAb

MC-38 cells (1.0×10^6) were injected subcutaneously into $Foxp3^{Thy1.1}$ C57BL/6 mice on day 0 (N = 6). TILs on day 12 were subjected to FCM.

(A and B) The uptake and content of FFAs in TILs were assessed with BODIPY FL C16 and BODIPY 493, respectively. Representative histogram plots (A) and MFI summary (B) are shown.

(C) The expression of fatty acid metabolism-related genes (*CD36*, *CPT1A*, *PPARA*, and *PPARG*) in TILs was examined by real-time qRT-PCR.

(legend continued on next page)

Immunity
Article

CellPress

tumors, whereas the numbers of CD8$^+$ T cells and conv CD4$^+$ T cells were lower (Figures 5A–5C). The abundant Treg cells in the TME of *RHOA* Y42C tumors were because of a less apoptotic and more proliferative nature compared with *RHOA* WT tumors (Figures S2H–S2M). In addition, Treg cells took in a larger amount of FFAs, and the expression of molecules related to FFA uptake and metabolism by tumor-infiltrating Treg cells was higher in *RHOA* Y42C tumors than in *RHOA* WT tumors (Figures 5D–5G).

We next examined the immunological phenotypes of Treg cells in the TME. The expression of activation markers by Treg cells in the TME was higher in the MC-38^{Y42C} tumors than in the MC-38^{WT} tumors in accordance with the data of human GC (Figures 1D, 1E, 5H, 5I, S1E, and S1F). Antigen-presenting cells (APCs) are an important target of Treg cells, as previously reported (Maeda et al., 2014; Qureshi et al., 2011; Wing et al., 2008). The expression of CD80 and CD86 by APCs in the TME was decreased in the MC-38^{Y42C} tumors (Figures 5J and 5K). Overall, abundant FFAs in the TME of tumors with *RHOA* Y42C contribute to compelling not only the survival, but also the immunosuppressive function of Treg cells.

Tumors with *RHOA* Y42 Mutaitons Respond to Therapy Combining PD-1 Blockade and a PI3Kβ Inhibitor

Tumor growth was comparable between *RHOA* WT and *RHOA* Y42C tumors in immunocompetent and immunocompromised mice, while differences in immunological phenotypes of TILs were detected according to the alteration of the *RHOA* gene (Figures S4A–S4C). We then addressed the antitumor efficacy of anti-PD-1 mAb *in vivo*. Anti-PD-1 mAb failed to inhibit the growth of *RHOA* Y42C tumors compared with that of *RHOA* WT tumors (Figures 6A, S4D, S5A, and S5B). The frequencies of MuLV-15E tetramer$^+$, CD62L$^-$CD44$^+$, tumor necrosis factor (TNF)-α$^+$ interferon (IFN)-γ$^+$, CD69$^+$, and Granzyme B$^+$ tumor-infiltrating CD8$^+$ T cells were increased by anti-PD-1 mAb in MC-38^{WT} tumors, but not in MC-38^{Y42C} tumors (Figures 6B, 6C, and S4E–S4L). We also evaluated the efficacy of anti-PD-1 mAb in three patients with advance GC that bore *RHOA* Y42 mutations (Table S4). None of these responded to anti-PD-1 mAb, and one patient experienced progressive disease after one course of anti-PD-1 mAb therapy (Figure S4N).

To elucidate the importance of abundant FFAs in the TME derived from the *RHOA* Y42C in the resistance to PD-1 blockade,

we addressed whether decreased expression of *Fasn* (Fasn^{RNAi}) or CD36 blockade recovered the antitumor efficacy of anti-PD-1 mAb in *RHOA* Y42C tumors. Treg cells, in addition to CTLA-4 expression, were decreased in Fasn^{RNAi} MC-38^{Y42C} tumors in number, while Foxp3$^-$CD4$^+$ T cells and CD8$^+$ T cells were increased (Figures 6D–6J). Accordingly, the tumor growth of Fasn^{RNAi} MC-38^{Y42C} was inhibited by anti-PD-1 mAb (Figure 6K and S4M). We next performed CD36 blockade to inhibit FFA transport. Anti-CD36 mAb decreased the number of Treg cells, as well as their CTLA-4 expression in MC-38^{Y42C} tumors, leading to the increase in Foxp3$^-$CD4$^+$ T cells and CD8$^+$ T cells (Figures 6L–6P). The antitumor efficacy of anti-PD-1 mAb was also improved by the combination with CD36 blockade (Figure 6Q, S5C, and S5D). Together with the data of *Fasn*-expressing MC-38 cell line (Figure 4Q), abundant FFAs in the TME derived from *RHOA* Y42C inhibit the antitumor efficacy of anti-PD-1 mAb.

We then hypothesized that inhibiting PI3K-AKT signaling pathways in *RHOA* Y42-mutated tumors could overcome the resistance to anti-PD-1 mAb treatment because PI3K-AKT signaling pathways play important roles in this immunosuppressive TME developed by *RHOA* Y42 mutations. While the inhibition of PI3K-AKT signaling pathways may influence the viabilities of immune cells (Fruman et al., 2017), the PI3Kβ isoform can regulate PI3K-AKT signaling pathways in tumors with PTEN deficiency without directly affecting Treg cell development, maintenance, or proliferation (Jia et al., 2008; Sauer et al., 2008). We then employed a selective PI3Kβ small-molecule inhibitor, GSK2636771, to address whether modulating PI3K-AKT signaling pathways could overcome the immunosuppressive phenotype. GSK2636771 inhibited AKT phosphorylation in a concentration-dependent manner, mainly in *RHOA* Y42C cancer cells, resulting in increased IRF1, CXCL10, and CXCL11 expression and decreased FAS expression *in vitro* (Figures S6A–S6D). Additionally, GSK2636771 reduced total FFA production from *RHOA* Y42C cancer cells (Figures S6E and S6F). Moreover, GSK2636771 decreased Treg cells and increased CD8$^+$ T cells in the TME of MC-38^{Y42C} tumors (Figures 7A–7C). The expression of activation markers on Treg cells was decreased (Figures 7D and 7E). The maturation of tumor-infiltrating APCs was improved by GSK2636771 (Figures 7F and 7G).

Next, the antitumor efficacy of anti-PD-1 mAb combined with GSK2636771 was examined. Each monotherapy hardly inhibited

---

(D and E) The expression of FFA metabolism-related molecules (CD36, CPT1A, PPARα, and PPARγ) in TILs was analyzed with FCM. Representative histogram plots (D) and MFI summary (E) are shown (N = 6).

(F and G) The uptake and content of FFAs in TILs from human GC clinical samples were analyzed with BODIPY FL C16 and BODIPY 493, respectively (N = 5). Representative histogram plots (F) and MFI summary (G) are shown.

(H and I) MC-38 cells (1.0×10^6) were injected subcutaneously into *Foxp3*$^{Thy1.1}$ C57BL/6 mice on day 0 (N = 6). TILs on day 12 were subjected to FCM. Glucose uptake (2-NBDG) and GLUT1 expression in TILs were assessed. Representative histogram plots (H) and MFI summaries (I) are shown.

(J) Mock or *Fasn* was retrovirally transduced into MC-38 cells. Representative blots of FAS from three independent experiments are shown.

(K–P) MC-38^{mock} or MC-38^{Fasn} cells (1.0×10^6) were injected subcutaneously into C57BL/6 mice on day 0. Tumor interstitial fluids or TILs were extracted from the MC-38^{mock} or MC-38^{Fasn} tumors on day 12. (K) Total FFAs in the interstitial fluids of the MC-38^{mock} or MC-38^{Fasn} tumors were evaluated by the Free Fatty Acid Quantification Kit (N = 4 per group). (L–P) TILs on day 12 were subjected to FCM. (L–N) The frequencies of Foxp3$^+$CD4$^+$ T cells, the ratio of Foxp3$^+$CD4$^+$ to CD8$^+$ T cells in the TME, and the number of each T cell subset (counts per tumor weight) were examined with FCM (N = 12 per group). Representative contour plots (L) and summary (M and N) are shown. (O and P) CTLA-4 expression by Foxp3$^+$CD4$^+$ T cells in the TME was examined with FCM (N = 6 per group). Representative histograms (O) and MFI summary (P) are shown.

(Q) MC-38^{mock} or MC-38^{Fasn} cells (1.0×10^6) were injected subcutaneously into C57BL/6 mice on day 0, and anti-PD-1 mAb or control mAb was administered on days 6, 11, and 16 (N = 12 per group). The tumor growth curves of the indicated groups are shown. NC, negative control; bars, mean; error bars, SEM; *p < 0.05; and **p < 0.01.
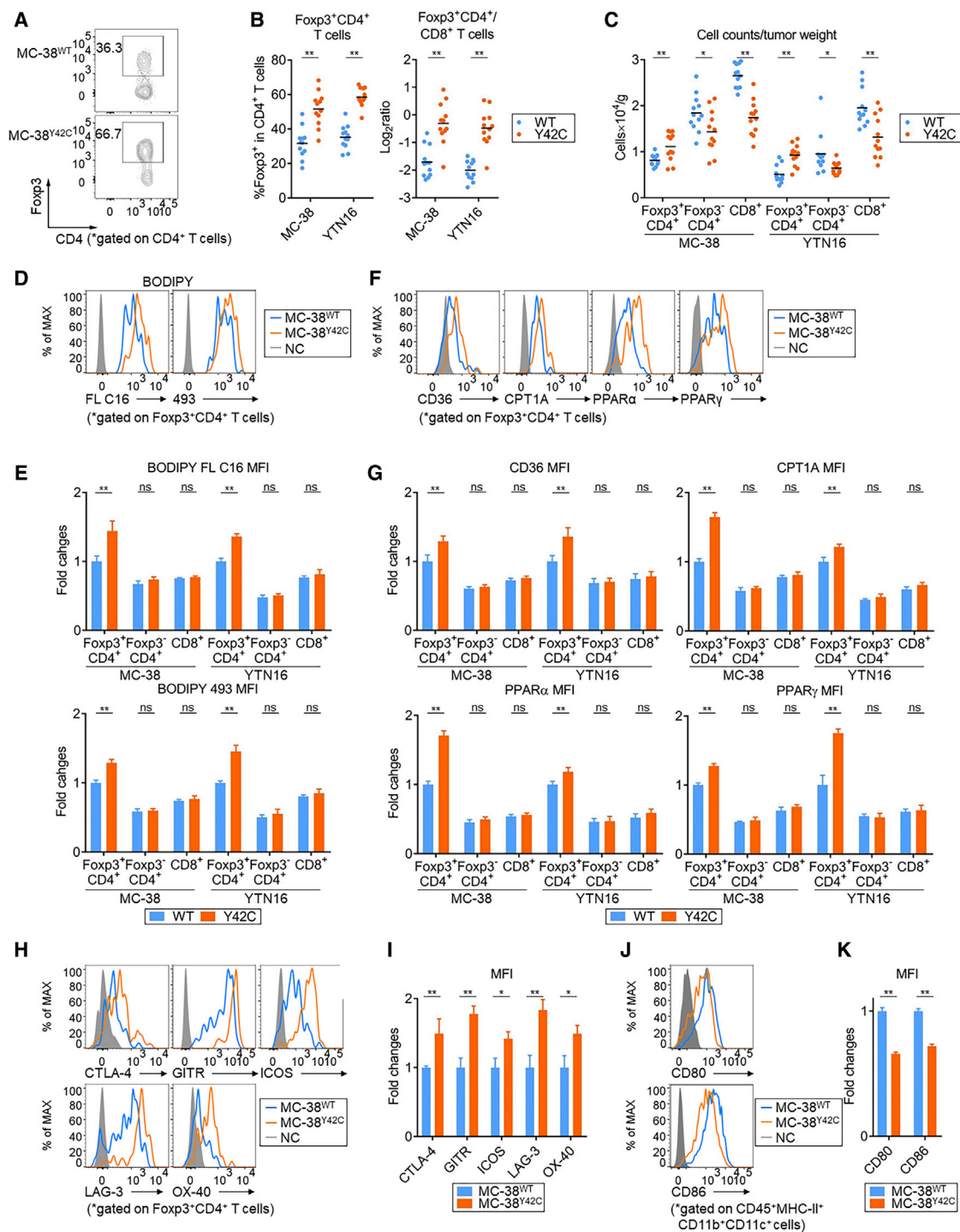
Figure 5. RHOA Y42 Mutations Promote the Development of an Immunosuppressive TME

RHOA WT or *RHOA* Y42C was retrovirally transduced into a murine gastric cancer cell line (YTN16^WT and YTN16^Y42C, respectively).

(A–C) MC-38^WT, MC-38^Y42C cells, YTN16^WT, or YTN16^Y42C (1.0 × 10^6) cells were injected subcutaneously into C57BL/6 mice on day 0. TILs on day 12 were subjected to FCM. The frequencies of Foxp3^+CD4^+ T cells, the ratio of Foxp3^+CD4^+ to CD8^+ T cells in the TME, and the number of each T cell subset (counts per tumor weight) were examined with FCM (N = 12 per group). Representative contour plots (A) and summaries (B and C) are shown.

(D and E) MC-38^WT, MC-38^Y42C, YTN16^WT, or YTN16^Y42C cells (1.0 × 10^6) were injected subcutaneously into *Foxp3*^Thy1.1 C57BL/6 mice on day 0 (MC-38^WT and MC-38^Y42C; N = 3, YTN16^WT and YTN16^Y42C; N = 5). TILs on day 12 were subjected to FCM. The uptake and content of FFAs in TILs were assessed with BODIPY FL C16 and BODIPY 493, respectively. Representative histogram plots (D) and MFI summaries (E) are shown.

(legend continued on next page)

CellPress

tumor growth, but combined treatment with GSK2636771 and anti-PD-1 mAb delayed MC-38^{Y42C} tumor growth and activated tumor-infiltrating CD8$^+$ T cells (Figures 7H–7J, S5E, S5F, and S7A–S7H). In contrast to the MC-38^{Y42C} tumors, MC-38^{WT} tumors showed no notable immunological changes in the TME by GSK2636771, resulting in no combination efficacy (Figures S7I–S7O). Given the importance of controlling Treg cells in the TME, we assessed whether anti-CTLA-4 mAb, which depletes Treg cells (Selby et al., 2013; Simpson et al., 2013; Wing et al., 2008), augmented the efficacy of anti-PD-1 mAb in MC-38^{Y42C} tumors. The combination treatment slowed the tumor growth compared with single mAb treatment (Figure 7K, S5G, and S5H). We propose that tumors with *RHOA* Y42 mutations are resistant to PD-1 blockade as a monotherapy because of the immunosuppressive TME, which can be overcome by the combination with a PI3Kβ inhibitor or Treg cell-targeted treatment such as anti-CTLA-4 mAb.

DISCUSSION

In this study, we revealed that a subset of GC exhibited an immunosuppressive TME that was characterized the accumulation of Treg cells in the absence of other inflammatory features. Some of these tumors harbored mutations in *RHOA*, including *RHOA* Y42C, a driver mutation in GC that accounts for 10%–25% of diffuse-type GCs (Cancer Genome Atlas Research Network., 2014; Kakiuchi et al., 2014; Wang et al., 2014). *RHOA* Y42-mutated GCs harbored a low TMB and inhibited effector T cell infiltration into the TME by decreasing IRF1 expression through PI3K-AKT signaling pathways, resulting in decreased production of the effector T cell-recruiting chemokines CXCL10 and CXCL11. On the other hand, higher tumor infiltration of Treg cells was not strongly correlated with the expression of Treg cell-recruiting chemokines; rather, the *RHOA* Y42 mutation induced abundant FFA production via the PI3K-AKT signaling pathways. This metabolic profile resulted in enhanced eTreg cell survival and immunosuppressive function in an FFA dose-dependent manner since Treg cells rely on mitochondrial metabolism to maintain immunoregulatory gene expression and immunosuppressive function, while effector T cells rely on a different metabolic profile (Angelin et al., 2017; Wang et al., 2017).

We demonstrated an immunological influence of *RHOA* Y42C on inhibiting CD8$^+$ T cell infiltration by changing the chemokine milieu in the TME via activating PI3K-AKT signaling pathways. Similar immunological influence has been reported in tumors harboring alterations in FAK, PTEN, EGFR, and WNT-β-catenin that all showed poor responses to ICB therapy (Jiang et al., 2016; Peng et al., 2016; Spranger et al., 2015). Particularly, activating PI3K-AKT signaling pathways are involved in *EGFR* mutations (Sugiyama et al., 2020) and *PTEN* loss (Peng et al., 2016). In fact, we found that *RHOA* Y42-mutated GCs exhibited a limited

clinical response to PD-1 blockade therapies, while PD-1 blockade therapies demonstrate clinical efficacy in unresectable advanced or recurrent GCs with response rates of 10%–25% (Kang et al., 2017). In line with this, diffuse-type GCs, as which *RHOA* Y42-mutated GCs are basically classified, are resistant to PD-1 blockade therapies (Kang et al., 2017). Therefore, our data can be applied for stratifying patients eligible for PD-1 blockade therapies via excluding a plausible non-responder population, leading to the improvement in response rates of ICB in GCs. In addition, Treg cell infiltration can be reportedly related to hyperprogressive disease by PD-1 blockade therapies (Kamada et al., 2019), further suggesting that *RHOA*-mutated GCs are not good candidates for PD-1 blockade monotherapy. Other types of malignancies with *RHOA* mutations that enhance PI3K-AKT signaling pathways may also provide the similar immunosuppressive effect (Yoo et al., 2014).

Various types of PI3K inhibitors have been tested in clinical trials involving patients with a wide range of cancers (Janku et al., 2018). Among these inhibitors, PI3Kδ inhibitors have been approved for clinical application by the U.S. Food and Drug Administration (FDA) (Janku et al., 2018), but the inactivation of p110δ in T cells may impair the differentiation of effector CD4$^+$ T cells (Okkenhaug et al., 2006; Soond et al., 2010) and CD8$^+$ T cells (Macintyre et al., 2011) as well as the functions of Treg cells (Ali et al., 2014; Patton et al., 2006). In contrast, treatment with a PI3Kβ inhibitor provides little impact on immune cells (Peng et al., 2016). We employed a PI3Kβ inhibitor to inhibit PI3K-AKT signaling pathways activated by *RHOA* Y42C in combination with ICB, leading to a far stronger antitumor effect than that produced by ICB alone. Thus, the PI3Kβ inhibitor could become a promising combination therapy with ICB in *RHOA* Y42-mutated malignancies and other types of gene alterations activating PI3K-AKT signaling pathways.

Foxp3 expression is involved in various metabolic programs, and Foxp3$^+$ Treg cells maintain high levels of AMPK activation, contributing to the high reliance on lipid oxidation (Angelin et al., 2017; Gerriets et al., 2016; Michalek et al., 2011; Muroski et al., 2017). Abundant FFA production by PI3K-AKT-mTOR signaling pathways provided a metabolic advantage for the survival and immunosuppressive function of Treg cells. The higher concentration of FFAs in the TME in *RHOA* Y42-mutated GCs enhanced survival and immunosuppressive function of Treg cells even in low-glucose environments. Additionally, a similar TME with abundant FFAs is reported in *Kras*-mutated cancers (Gouw et al., 2017), suggesting that the mechanism of metabolic advantage by driver gene mutations observed in our study may be a common system for developing an immunosuppressive TME. The glucose deprivation in the TME, which is lethal to CD8$^+$ T cells and FOXP3$^-$CD4$^+$ T cells, may have minimal influences on eTreg cells. Yet, it has not been determined whether fatty acid production by cancer cells is sufficient for Treg cell

---

(F–K) MC-38^{WT}, MC-38^{Y42C} (F–K), YTN16^{WT}, or YTN16^{Y42C} cells (F and G) (1.0 × 10^6) were injected subcutaneously into C57BL/6 mice on day 0 (MC-38^{WT} and MC-38^{Y42C}; N = 3, YTN16^{WT} and YTN16^{Y42C}; N = 5). TILs prepared from tumor tissue samples on day 12 were subjected to FCM. The expression of fatty acid metabolism-related molecules (CD36, CPT1A, PPARα, and PPARγ) in TILs was analyzed with FCM. Representative histogram plots (F) and MFI summaries (G) are shown. (H and I) The expression of CTLA-4, GITR, ICOS, LAG-3, and OX-40 by Foxp3$^+$CD4$^+$ T cells in the TME was examined with FCM (N = 6 per group). Representative histograms (H) and MFI summaries (I) are shown. (J and K) The expression of CD80 and CD86 by tumor-infiltrating APCs (detected as CD45$^+$MHC-II$^+$CD11b$^+$CD11c$^+$ cells) was analyzed (N = 6 per group). Representative histogram plots (J) and MFI summaries (K) are shown. NC, negative control; bars, mean; error bars, SEM; *p < 0.05; **p < 0.01; and ns, not significant.
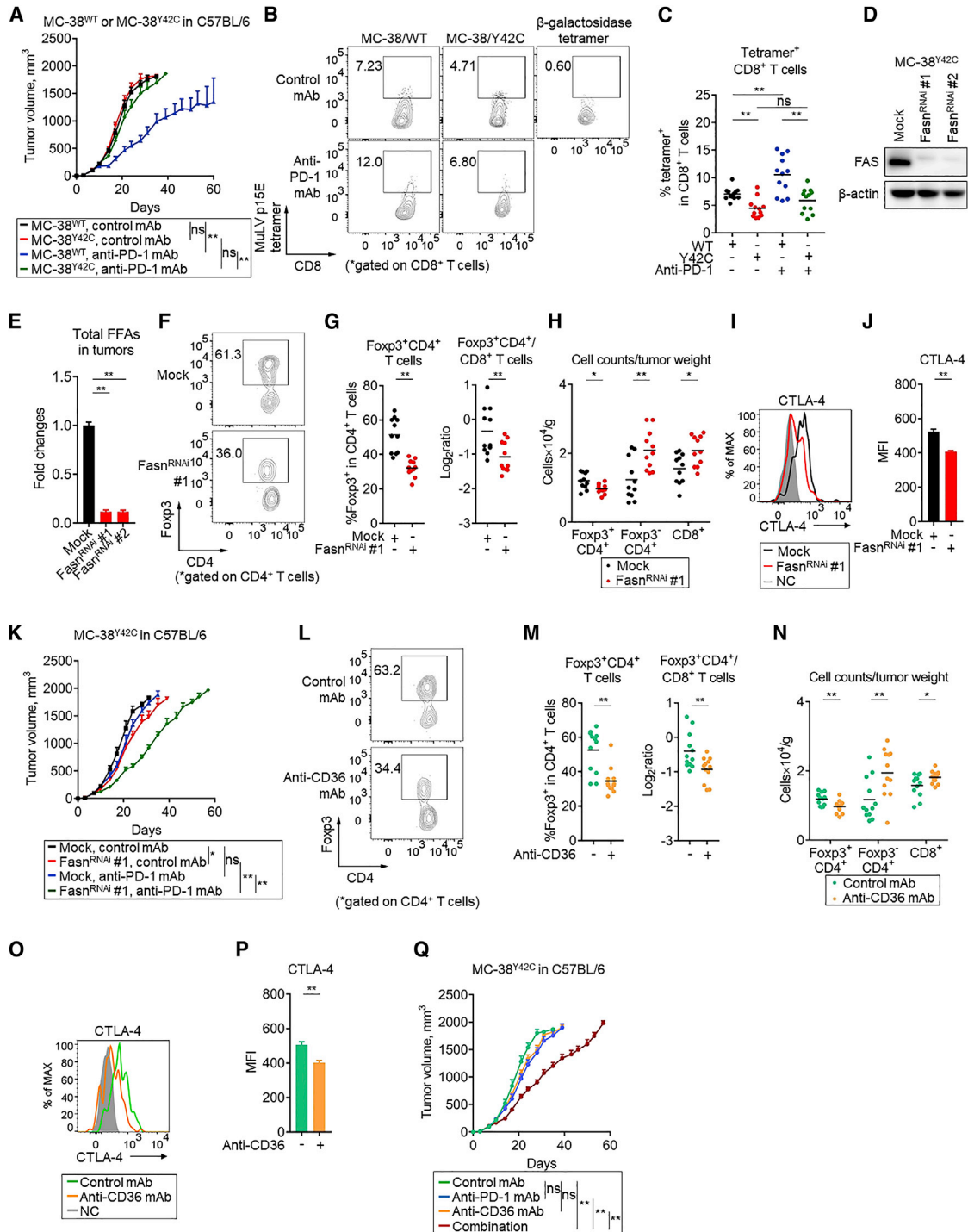
Figure 6. Abundant FFAs in *RHOA* Y42-Mutated Tumors Induce the Resistance to Anti-PD-1 mAb Treatment

(A–C) MC-38^{WT} or MC-38^{Y42C} cells (1.0 × 10^6) were injected subcutaneously into C57BL/6 mice on day 0, and anti-PD-1 mAb or control mAb was administered on days 6, 11, and 16 (N = 12 per group). The tumor growth curves of the indicated groups are shown in (A). TILs on day 12 were subjected to FCM. MC-38 antigen-specific CD8$^+$ T cells were detected by MuLV p15E/H-2Kb tetramers (N = 12 per group). Representative contour plots (B) and summary (C) are shown. β-galactosidase/H-2Kb tetramer staining served as a control.

(D–K) Mock or Fasn^{RNAi} was lentivirally transduced into MC-38^{Y42C} cells. Representative blots of FAS from three independent experiments are shown (D). (E–J) Mock MC-38^{Y42C} or Fasn^{RNAi} MC-38^{Y42C} cells (1.0 × 10^6) were injected subcutaneously into C57BL/6 mice on day 0. Tumor interstitial fluids or TILs were extracted from the Mock MC-38^{Y42C} or Fasn^{RNAi} MC-38^{Y42C} tumors on day 12. (E) Total FFAs in the interstitial fluids of the Mock MC-38^{Y42C} or Fasn^{RNAi} MC-38^{Y42C} tumors were evaluated by the Free Fatty Acid Quantification Kit (N = 4 per group). (F–J) TILs on day 12 were subjected to FCM. The frequencies of Foxp3$^+$CD4$^+$ T cells, the ratio of Foxp3$^+$CD4$^+$ to CD8$^+$ T cells in the TME, and the number of each T cell subsets (cell counts per tumor weight) were examined with FCM (N = 11

(legend continued on next page)

Immunity
Article

🔵 **CellPress**

survival and immunosuppressive function, while increased fatty acid production in cancer cells may increase lipid availability in the TME (Röhrig and Schulze, 2016). We showed that eTreg cells could take in larger amount of FFAs provided by the *RHOA* Y42-mutated tumors and more effectively employ lipid metabolism pathways for their survival and immunosuppressive functions than could other T cell subsets in the TME. This means that FFA doses in the TME can reflect the survival and immunosuppressive function of Treg cells. Nevertheless, some reports show a crucial role for aerobic glycolysis in Treg cells, as observed in effector T cells (Fan and Turka, 2018; Gerriets et al., 2016; Kishore et al., 2017; Li et al., 2019; Procaccini et al., 2016). These contradictory findings may be partially due to anatomical location. Indeed, tissue-resident Treg cells that localize in nonlymphoid tissues, such as the visceral adipose tissue, are highly dependent on lipid metabolism (Cipolletta et al., 2012). Treg cells therefore have a more redundant metabolic profile than other T cell subsets and can survive and function even in low-glucose and hypoxic conditions like TMEs.

In conclusion, we found that *RHOA* mutations establish an immunosuppressive TME characterized by eTreg cell infiltration regardless of the non-inflammatory TME in humans. The immunosuppressive microenvironment of *RHOA* Y42-mutated GCs is induced by reduced levels of effector T cell-recruiting chemokines and increased production of FFAs via the activation of PI3K-AKT signaling pathways: eTreg cells survive and function with FFA metabolism, while glucose deprivation is lethal to $CD8^+$ T cells and conventional $CD4^+$ T cells. We thus propose that driver gene alterations are essential not only in the proliferation and survival of cancer cells, but also in the development of an immune escape-enabling TME, warranting further evaluation of cancer immunotherapies combined with molecular-targeted therapies against driver gene alterations.

STAR★METHODS

Detailed methods are provided in the online version of this paper and include the following:

SUPPLEMENTAL INFORMATION

Supplemental Information can be found online at https://doi.org/10.1016/j.immuni.2020.06.016.

per group). The expression of CTLA-4 by $Foxp3^+CD4^+$ T cells in the TME was examined with FCM (N = 6 per group). Representative contour plots (F) or histograms (I) and summaries (G, H, and J) are shown. (K) Mock $MC-38^{Y42C}$ or $Fasn^{RNAi}$ $MC-38^{Y42C}$ cells (1.0×10^6) were injected subcutaneously into C57BL/6 mice on day 0, and anti-PD-1 mAb or control mAb was administered on days 6, 11, and 16 (N = 12 per group). The tumor growth curves of the indicated groups are shown.

(L–P) $MC-38^{Y42C}$ cells (1.0×10^6) were injected subcutaneously into C57BL/6 mice on day 0. Anti-CD36 mAb or control mAb was administered daily (N = 12 per group). TILs prepared from tumor tissue samples on day 12 were subjected to FCM. (L–N) The frequencies of $Foxp3^+CD4^+$ T cells, the ratio of $Foxp3^+CD4^+$ to $CD8^+$ T cells in the TME, and the number of each T cell subsets (cell counts per tumor weight) were examined with FCM (N = 12 per group). The expression of CTLA-4 by $Foxp3^+CD4^+$ T cells in the TME was examined with FCM (N = 6 per group). Representative contour plots or histograms (L and O) and summaries (M, N, and P) are shown.

(Q) $MC-38^{Y42C}$ cells (1.0×10^6) were injected subcutaneously into C57BL/6 mice on day 0, and anti-PD-1 mAb (intravenously, on days 6, 11, and 16) and/or anti-CD36 mAb (intravenously, daily) was administered (N = 12 per group). The tumor growth curves of the indicated groups are shown. NC, negative control; bars, mean; error bars, SEM; *$p < 0.05$; **$p < 0.01$; and ns, not significant.
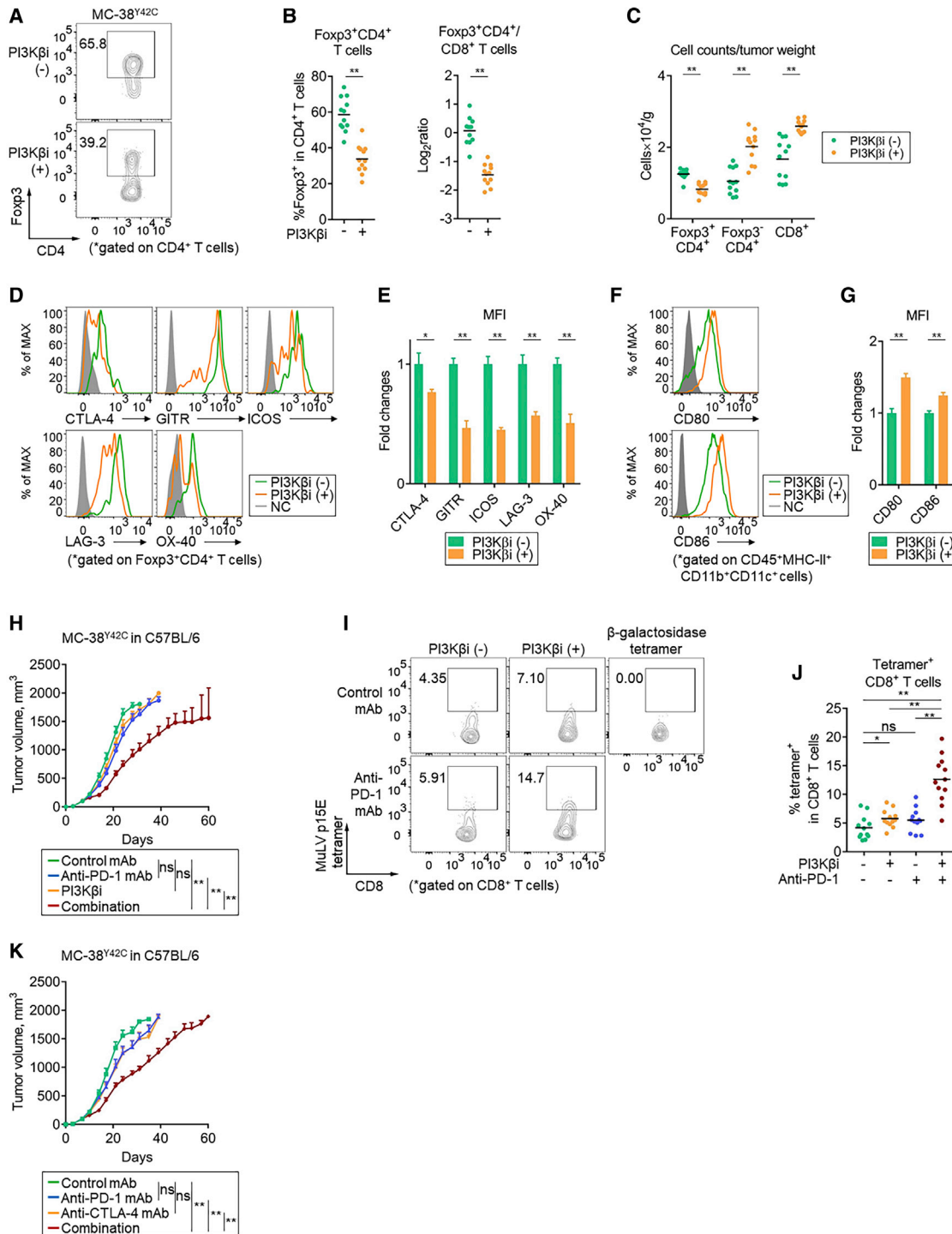
Figure 7. The Combination with a PI3Kβ Inhibitor or Anti-CTLA-4 mAb Overcomes the Resistance of _RHOA_ Y42-Mutated Tumors to Anti-PD-1 mAb

(A–G) MC-38^{Y42C} cells (1.0×10^6) were injected subcutaneously into C57BL/6 mice on day 0, and GSK2636771 was orally administered for 5 days. TILs on day 12 were subjected to FCM. Representative contour plots for CD4 and Foxp3 (A) and summaries (B and C) are shown (N = 12 per group). (D and E) The expression of CTLA-4, GITR, ICOS, LAG-3, and OX-40 by Foxp3$^+$CD4$^+$ T cells in the TME was evaluated (N = 6 per group). Representative histogram plots (D) and MFI summaries are shown (E). (F and G) The expression of CD80 and CD86 by APCs in the TME was examined (N = 6 per group). Representative histogram plots (F) and MFI summaries (G) are shown.

(legend continued on next page)

Immunity
Article

CellPress

REFERENCES

Ali, K., Soond, D.R., Pineiro, R., Hagemann, T., Pearce, W., Lim, E.L., Bouabe, H., Scudamore, C.L., Hancox, T., Maecker, H., et al. (2014). Inactivation of PI(3) K p110δ breaks regulatory T-cell-mediated immune tolerance to cancer. Nature 510, 407–411.

Angelin, A., Gil-de-Gómez, L., Dahiya, S., Jiao, J., Guo, L., Levine, M.H., Wang, Z., Quinn, W.J., 3rd, Kopinski, P.K., Wang, L., et al. (2017). Foxp3 Reprograms T Cell Metabolism to Function in Low-Glucose, High-Lactate Environments. Cell Metab. 25, 1282–1293.

Ayers, M., Lunceford, J., Nebozhyn, M., Murphy, E., Loboda, A., Kaufman, D.R., Albright, A., Cheng, J.D., Kang, S.P., Shankaran, V., et al. (2017). IFN-γ-related mRNA profile predicts clinical response to PD-1 blockade. J. Clin. Invest. 127, 2930–2940.

Bae, C.D., Min, D.S., Fleming, I.N., and Exton, J.H. (1998). Determination of interaction sites on the small G protein RhoA for phospholipase D. J. Biol. Chem. 273, 11596–11604.

Borghaei, H., Paz-Ares, L., Horn, L., Spigel, D.R., Steins, M., Ready, N.E., Chow, L.Q., Vokes, E.E., Felip, E., Holgado, E., et al. (2015). Nivolumab versus Docetaxel in Advanced Nonsquamous Non-Small-Cell Lung Cancer. N. Engl. J. Med. 373, 1627–1639.

Cancer Genome Atlas Research Network (2014). Comprehensive molecular characterization of gastric adenocarcinoma. Nature 513, 202–209.

Chang, C.H., Qiu, J., O'Sullivan, D., Buck, M.D., Noguchi, T., Curtis, J.D., Chen, Q., Gindin, M., Gubin, M.M., van der Windt, G.J., et al. (2015). Metabolic Competition in the Tumor Microenvironment Is a Driver of Cancer Progression. Cell 162, 1229–1241.

Cipolletta, D., Feuerer, M., Li, A., Kamei, N., Lee, J., Shoelson, S.E., Benoist, C., and Mathis, D. (2012). PPAR-γ is a major driver of the accumulation and phenotype of adipose tissue Treg cells. Nature 486, 549–553.

Curiel, T.J., Coukos, G., Zou, L., Alvarez, X., Cheng, P., Mottram, P., Evdemon-Hogan, M., Conejo-Garcia, J.R., Zhang, L., Burow, M., et al. (2004). Specific recruitment of regulatory T cells in ovarian carcinoma fosters immune privilege and predicts reduced survival. Nat. Med. 10, 942–949.

Currie, E., Schulze, A., Zechner, R., Walther, T.C., and Farese, R.V., Jr. (2013). Cellular fatty acid metabolism and cancer. Cell Metab. 18, 153–161.

Düvel, K., Yecies, J.L., Menon, S., Raman, P., Lipovsky, A.I., Souza, A.L., Triantafellow, E., Ma, Q., Gorski, R., Cleaver, S., et al. (2010). Activation of a metabolic gene regulatory network downstream of mTOR complex 1. Mol. Cell 39, 171–183.

Fan, M.Y., and Turka, L.A. (2018). Immunometabolism and PI(3)K Signaling As a Link between IL-2, Foxp3 Expression, and Suppressor Function in Regulatory T Cells. Front. Immunol. 9, 69.

Fridman, W.H., Pagès, F., Sautès-Fridman, C., and Galon, J. (2012). The immune contexture in human tumours: impact on clinical outcome. Nat. Rev. Cancer 12, 298–306.

Fruman, D.A., Chiu, H., Hopkins, B.D., Bagrodia, S., Cantley, L.C., and Abraham, R.T. (2017). The PI3K Pathway in Human Disease. Cell 170, 605–635.

Gatenby, R.A., and Gillies, R.J. (2004). Why do cancers have high aerobic glycolysis? Nat. Rev. Cancer 4, 891–899.

Gerriets, V.A., Kishton, R.J., Johnson, M.O., Cohen, S., Siska, P.J., Nichols, A.G., Warmoes, M.O., de Cubas, A.A., MacIver, N.J., Locasale, J.W., et al. (2016). Foxp3 and Toll-like receptor signaling balance T_{reg} cell anabolic metabolism for suppression. Nat. Immunol. 17, 1459–1466.

Gorbachev, A.V., Kobayashi, H., Kudo, D., Tannenbaum, C.S., Finke, J.H., Shu, S., Farber, J.M., and Fairchild, R.L. (2007). CXC chemokine ligand 9/ monokine induced by IFN-gamma production by tumor cells is critical for T cell-mediated suppression of cutaneous tumors. J Immunol. 178, 2278–2286.

Gouw, A.M., Eberlin, L.S., Margulis, K., Sullivan, D.K., Toal, G.G., Tong, L., Zare, R.N., and Felsher, D.W. (2017). Oncogene KRAS activates fatty acid synthase, resulting in specific ERK and lipid signatures associated with lung adenocarcinoma. Proc. Natl. Acad. Sci. USA 114, 4300–4305.

Griffith, J.W., Sokol, C.L., and Luster, A.D. (2014). Chemokines and chemokine receptors: positioning cells for host defense and immunity. Annu. Rev. Immunol. 32, 659–702.

Harikumar, K.B., Yester, J.W., Surace, M.J., Oyeniran, C., Price, M.M., Huang, W.C., Hait, N.C., Allegood, J.C., Yamada, A., Kong, X., et al. (2014). K63-linked polyubiquitination of transcription factor IRF1 is essential for IL-1-induced production of chemokines CXCL10 and CCL5. Nat. Immunol. 15, 231–238.

Hensbergen, P.J., Wijnands, P.G., Schreurs, M.W., Scheper, R.J., Willemze, R., and Tensen, C.P. (2005). The CXCR3 targeting chemokine CXCL11 has potent antitumor activity in vivo involving attraction of CD8^{+} T lymphocytes but not inhibition of angiogenesis. J Immunother. 28, 343–351.

Ho, P.C., and Kaech, S.M. (2017). Reenergizing T cell anti-tumor immunity by harnessing immunometabolic checkpoints and machineries. Curr. Opin. Immunol. 46, 38–44.

(H–J) MC-38^{Y42C} cells (1.0×10^6) were injected subcutaneously into C57BL/6 mice on day 0. The mice were treated with anti-PD-1 mAb (intravenously, on days 6, 11, and 16) and/or GSK2636771 (orally, for 5 days) (N = 12 per group). The tumor growth curves of the indicated groups are shown in (H). TILs were prepared from tumor tissue samples on day 12, and tumor antigen-specific CD8^{+} T cells were detected by MuLV p15E/H-2Kb tetramers (N = 12 per group). Representative contour plots (I) and summary (J) are shown. β-galactosidase/H-2Kb tetramer staining served as a control.

(K) MC-38^{Y42C} cells (1.0×10^6) were injected subcutaneously into C57BL/6 mice on day 0. These mice were treated with anti-PD-1 mAb (intravenously, on days 6, 11, and 16) and/or anti-CTLA-4 mAb (intravenously, on days 6, 11, and 16) (N = 12 per group). The tumor growth curves of the indicated groups are shown. NC, negative control; bars, mean; error bars, SEM; PI3Kβi, PI3Kβ inhibitor; $p < 0.05$; $p < 0.01$; and ns, not significant.

Hoelzinger, D.B., Smith, S.E., Mirza, N., Dominguez, A.L., Manrique, S.Z., and Lustgarten, J. (2010). Blockade of CCL1 inhibits T regulatory cell suppressive function enhancing tumor immunity without affecting T effector responses. J Immunol. 184, 6833–6842.

Janku, F., Yap, T.A., and Meric-Bernstam, F. (2018). Targeting the PI3K pathway in cancer: are we making headway? Nat. Rev. Clin. Oncol. 15, 273–291.

Jia, S., Liu, Z., Zhang, S., Liu, P., Zhang, L., Lee, S.H., Zhang, J., Signoretti, S., Loda, M., Roberts, T.M., and Zhao, J.J. (2008). Essential roles of PI(3)K-p110beta in cell growth, metabolism and tumorigenesis. Nature 454, 776–779.

Jiang, H., Hegde, S., Knolhoff, B.L., Zhu, Y., Herndon, J.M., Meyer, M.A., Nywening, T.M., Hawkins, W.G., Shapiro, I.M., Weaver, D.T., et al. (2016). Targeting focal adhesion kinase renders pancreatic cancers responsive to checkpoint immunotherapy. Nat. Med. 22, 851–860.

Kakiuchi, M., Nishizawa, T., Ueda, H., Gotoh, K., Tanaka, A., Hayashi, A., Yamamoto, S., Tatsuno, K., Katoh, H., Watanabe, Y., et al. (2014). Recurrent gain-of-function mutations of RHOA in diffuse-type gastric carcinoma. Nat. Genet. 46, 583–587.

Kamada, T., Togashi, Y., Tay, C., Ha, D., Sasaki, A., Nakamura, Y., Sato, E., Fukuoka, S., Tada, Y., Tanaka, A., et al. (2019). PD-1+ regulatory T cells amplified by PD-1 blockade promote hyperprogression of cancer. Proc Natl Acad Sci USA. 116, 9999–10008.

Kang, Y.K., Boku, N., Satoh, T., Ryu, M.H., Chao, Y., Kato, K., Chung, H.C., Chen, J.S., Muro, K., Kang, W.K., et al. (2017). Nivolumab in patients with advanced gastric or gastro-oesophageal junction cancer refractory to, or intolerant of, at least two previous chemotherapy regimens (ONO-4538-12, ATTRACTION-2): a randomised, double-blind, placebo-controlled, phase 3 trial. Lancet 390, 2461–2471.

Kim, D., Pertea, G., Trapnell, C., Pimentel, H., Kelley, R., and Salzberg, S.L. (2013). TopHat2: accurate alignment of transcriptomes in the presence of insertions, deletions and gene fusions. Genome Biol. 14, R36.

Kishore, M., Cheung, K.C.P., Fu, H., Bonacina, F., Wang, G., Coe, D., Ward, E.J., Colamatteo, A., Jangani, M., Baragetti, A., et al. (2017). Regulatory T Cell Migration Is Dependent on Glucokinase-Mediated Glycolysis. Immunity 47, 875–889.

Li, H., and Durbin, R. (2009). Fast and accurate short read alignment with Burrows-Wheeler transform. Bioinformatics 25, 1754–1760.

Li, L., Liu, X., Sanders, K.L., Edwards, J.L., Ye, J., Si, F., Gao, A., Huang, L., Hsueh, E.C., Ford, D.A., et al. (2019). TLR8-Mediated Metabolic Control of Human Treg Function: A Mechanistic Target for Cancer Immunotherapy. Cell Metab. 29, 103–123.

Macintyre, A.N., Finlay, D., Preston, G., Sinclair, L.V., Waugh, C.M., Tamas, P., Feijoo, C., Okkenhaug, K., and Cantrell, D.A. (2011). Protein kinase B controls transcriptional programs that direct cytotoxic T cell fate but is dispensable for T cell metabolism. Immunity 34, 224–236.

Maeda, Y., Nishikawa, H., Sugiyama, D., Ha, D., Hamaguchi, M., Saito, T., Nishioka, M., Wing, J.B., Adeegbe, D., Katayama, I., and Sakaguchi, S. (2014). Detection of self-reactive CD8+ T cells with an anergic phenotype in healthy individuals. Science 346, 1536–1540.

Mantovani, A., Marchesi, F., Malesci, A., Laghi, L., and Allavena, P. (2017). Tumour-associated macrophages as treatment targets in oncology. Nat. Rev. Clin. Oncol. 14, 399–416.

Michalek, R.D., Gerriets, V.A., Jacobs, S.R., Macintyre, A.N., MacIver, N.J., Mason, E.F., Sullivan, S.A., Nichols, A.G., and Rathmell, J.C. (2011). Cutting edge: distinct glycolytic and lipid oxidative metabolic programs are essential for effector and regulatory CD4+ T cell subsets. J Immunol. 186, 3299–3303.

Miyara, M., Yoshioka, Y., Kitoh, A., Shima, T., Wing, K., Niwa, A., Parizot, C., Taflin, C., Heike, T., Valeyre, D., et al. (2009). Functional delineation and differentiation dynamics of human CD4+ T cells expressing the FoxP3 transcription factor. Immunity 30, 899–911.

Muraoka, D., Kato, T., Wang, L., Maeda, Y., Noguchi, T., Harada, N., Takeda, K., Yagita, H., Guillaume, P., Luescher, I., et al. (2010). Peptide vaccine induces enhanced tumor growth associated with apoptosis induction in CD8+ T cells. J Immunol. 185, 3768–3776.

Muroski, M.E., Miska, J., Chang, A.L., Zhang, P., Rashidi, A., Moore, H., Lopez-Rosas, A., Han, Y., and Lesniak, M.S. (2017). Fatty Acid Uptake in T Cell Subsets Using a Quantum Dot Fatty Acid Conjugate. Sci. Rep. 7, 5790.

Nagarsheth, N., Wicha, M.S., and Zou, W. (2017). Chemokines in the cancer microenvironment and their relevance in cancer immunotherapy. Nat. Rev. Immunol. 17, 559–572.

Okkenhaug, K., Patton, D.T., Bilancio, A., Garcon, F., Rowan, W.C., and Vanhaesebroeck, B. (2006). The p110delta isoform of phosphoinositide 3-kinase controls clonal expansion and differentiation of Th cells. J Immunol. 177, 5122–5128.

Patton, D.T., Garden, O.A., Pearce, W.P., Clough, L.E., Monk, C.R., Leung, E., Rowan, W.C., Sancho, S., Walker, L.S., Vanhaesebroeck, B., and Okkenhaug, K. (2006). Cutting edge: the phosphoinositide 3-kinase p110 delta is critical for the function of CD4+CD25+Foxp3+ regulatory T cells. J Immunol. 177, 6598–6602.

Peng, W., Chen, J.Q., Liu, C., Malu, S., Creasy, C., Tetzlaff, M.T., Xu, C., McKenzie, J.A., Zhang, C., Liang, X., et al. (2016). Loss of PTEN Promotes Resistance to T Cell-Mediated Immunotherapy. Cancer Discov. 6, 202–216.

Peterson, T.R., Sengupta, S.S., Harris, T.E., Carmack, A.E., Kang, S.A., Balderas, E., Guertin, D.A., Madden, K.L., Carpenter, A.E., Finck, B.N., and Sabatini, D.M. (2011). mTOR complex 1 regulates lipin 1 localization to control the SREBP pathway. Cell 146, 408–420.

Porstmann, T., Santos, C.R., Griffiths, B., Cully, M., Wu, M., Leevers, S., Griffiths, J.R., Chung, Y.L., and Schulze, A. (2008). SREBP activity is regulated by mTORC1 and contributes to Akt-dependent cell growth. Cell Metab. 8, 224–236.

Procaccini, C., Carbone, F., Di Silvestre, D., Brambilla, F., De Rosa, V., Galgani, M., Faicchia, D., Marone, G., Tramontano, D., Corona, M., et al. (2016). The Proteomic Landscape of Human Ex Vivo Regulatory and Conventional T Cells Reveals Specific Metabolic Requirements. Immunity 44, 406–421.

Qureshi, O.S., Zheng, Y., Nakamura, K., Attridge, K., Manzotti, C., Schmidt, E.M., Baker, J., Jeffery, L.E., Kaur, S., Briggs, Z., et al. (2011). Trans-endocytosis of CD80 and CD86: a molecular basis for the cell-extrinsic function of CTLA-4. Science 332, 600–603.

Ramana, C.V., Chatterjee-Kishore, M., Nguyen, H., and Stark, G.R. (2000). Complex roles of Stat1 in regulating gene expression. Oncogene 19, 2619–2627.

Reck, M., Rodríguez-Abreu, D., Robinson, A.G., Hui, R., Csőszi, T., Fülöp, A., Gottfried, M., Peled, N., Tafreshi, A., Cuffe, S., et al.; KEYNOTE-024 Investigators (2016). Pembrolizumab versus Chemotherapy for PD-L1-Positive Non-Small-Cell Lung Cancer. N. Engl. J. Med. 375, 1823–1833.

Rizvi, N.A., Hellmann, M.D., Snyder, A., Kvistborg, P., Makarov, V., Havel, J.J., Lee, W., Yuan, J., Wong, P., Ho, T.S., et al. (2015). Cancer immunology. Mutational landscape determines sensitivity to PD-1 blockade in non-small cell lung cancer. Science 348, 124–128.

Robert, C., Schachter, J., Long, G.V., Arance, A., Grob, J.J., Mortier, L., Daud, A., Carlino, M.S., McNeil, C., Lotem, M., et al.; KEYNOTE-006 investigators (2015). Pembrolizumab versus Ipilimumab in Advanced Melanoma. N. Engl. J. Med. 372, 2521–2532.

Röhrig, F., and Schulze, A. (2016). The multifaceted roles of fatty acid synthesis in cancer. Nat. Rev. Cancer 16, 732–749.

Rooney, M.S., Shukla, S.A., Wu, C.J., Getz, G., and Hacohen, N. (2015). Molecular and genetic properties of tumors associated with local immune cytolytic activity. Cell 160, 48–61.

Sahai, E., Alberts, A.S., and Treisman, R. (1998). RhoA effector mutants reveal distinct effector pathways for cytoskeletal reorganization, SRF activation and transformation. EMBO J. 17, 1350–1361.

Saito, T., Nishikawa, H., Wada, H., Nagano, Y., Sugiyama, D., Atarashi, K., Maeda, Y., Hamaguchi, M., Ohkura, N., Sato, E., et al. (2016). Two FOXP3+CD4+ T cell subpopulations distinctly control the prognosis of colorectal cancers. Nat. Med. 22, 679–684.

Sato, E., Olson, S.H., Ahn, J., Bundy, B., Nishikawa, H., Qian, F., Jungbluth, A.A., Frosina, D., Gnjatic, S., Ambrosone, C., et al. (2005). Intraepithelial

CellPress

CD8+ tumor-infiltrating lymphocytes and a high CD8+/regulatory T cell ratio are associated with favorable prognosis in ovarian cancer. Proc. Natl. Acad. Sci. USA 102, 18538–18543.

Sauer, S., Bruno, L., Hertweck, A., Finlay, D., Leleu, M., Spivakov, M., Knight, Z.A., Cobb, B.S., Cantrell, D., O'Connor, E., et al. (2008). T cell receptor signaling controls Foxp3 expression via PI3K, Akt, and mTOR. Proc. Natl. Acad. Sci. USA 105, 7797–7802.

Schachter, J., Ribas, A., Long, G.V., Arance, A., Grob, J.J., Mortier, L., Daud, A., Carlino, M.S., McNeil, C., Lotem, M., et al. (2017). Pembrolizumab versus ipilimumab for advanced melanoma: final overall survival results of a multi-centre, randomised, open-label phase 3 study (KEYNOTE-006). Lancet 390, 1853–1862.

Selby, M.J., Engelhardt, J.J., Quigley, M., Henning, K.A., Chen, T., Srinivasan, M., and Korman, A.J. (2013). Anti-CTLA-4 antibodies of IgG2a isotype enhance antitumor activity through reduction of intratumoral regulatory T cells. Cancer Immunol. Res. 1, 32–42.

Shitara, K., Özgüroğlu, M., Bang, Y.J., Di Bartolomeo, M., Mandalà, M., Ryu, M.H., Fornaro, L., Olesiński, T., Caglevic, C., Chung, H.C., et al.; KEYNOTE-061 investigators (2018). Pembrolizumab versus paclitaxel for previously treated, advanced gastric or gastro-oesophageal junction cancer (KEYNOTE-061): a randomised, open-label, controlled, phase 3 trial. Lancet 392, 123–133.

Simpson, T.R., Li, F., Montalvo-Ortiz, W., Sepulveda, M.A., Bergerhoff, K., Arce, F., Roddie, C., Henry, J.Y., Yagita, H., Wolchok, J.D., et al. (2013). Fc-dependent depletion of tumor-infiltrating regulatory T cells co-defines the efficacy of anti-CTLA-4 therapy against melanoma. J. Exp. Med. 210, 1695–1710.

Soond, D.R., Bjørgo, E., Moltu, K., Dale, V.Q., Patton, D.T., Torgersen, K.M., Galleway, F., Twomey, B., Clark, J., Gaston, J.S., et al. (2010). PI3K p110delta regulates T-cell cytokine production during primary and secondary immune responses in mice and humans. Blood 115, 2203–2213.

Spranger, S., Bao, R., and Gajewski, T.F. (2015). Melanoma-intrinsic β-catenin signalling prevents anti-tumour immunity. Nature 523, 231–235.

Spranger, S., Spaapen, R.M., Zha, Y., Williams, J., Meng, Y., Ha, T.T., and Gajewski, T.F. (2013). Up-regulation of PD-L1, IDO, and Tregs in the melanoma tumor microenvironment is driven by CD8+ T cells. Sci. Transl. Med. 5, 200ra116.

Subramanian, A., Tamayo, P., Mootha, V.K., Mukherjee, S., Ebert, B.L., Gillette, M.A., Paulovich, A., Pomeroy, S.L., Golub, T.R., Lander, E.S., and Mesirov, J.P. (2005). Gene set enrichment analysis: a knowledge-based approach for interpreting genome-wide expression profiles. Proc. Natl. Acad. Sci. USA 102, 15545–15550.

Sugiyama, E., Togashi, Y., Takeuchi, Y., Shinya, S., Tada, Y., Kataoka, K., Tane, K., Sato, E., Ishii, G., Goto, K., et al. (2020). Blockade of EGFR improves responsiveness to PD-1 blockade in EGFR-mutated non-small cell lung cancer. Sci. Immunol. 5, eaav3937.

Tada, Y., Togashi, Y., Kotani, D., Kuwata, T., Sato, E., Kawazoe, A., Doi, T., Wada, H., Nishikawa, H., and Shitara, K. (2018). Targeting VEGFR2 with Ramucirumab strongly impacts effector/ activated regulatory T cells and CD8+ T cells in the tumor microenvironment. J. Immunother. Cancer 6, 106.

Takeuchi, Y., Tanemura, A., Tada, Y., Katayama, I., Kumanogoh, A., and Nishikawa, H. (2018). Clinical response to PD-1 blockade correlates with a sub-fraction of peripheral central memory CD4+ T cells in patients with malignant melanoma. Int. Immunol. 30, 13–22.

Togashi, Y., Shitara, K., and Nishikawa, H. (2019). Regulatory T cells in cancer immunosuppression - implications for anticancer therapy. Nat. Rev. Clin. Oncol. 16, 356–371.

Tran, D.Q., Ramsey, H., and Shevach, E.M. (2007). Induction of FOXP3 expression in naive human CD4+FOXP3 T cells by T-cell receptor stimulation is transforming growth factor-beta dependent but does not confer a regulatory phenotype. Blood 110, 2983–2990.

Trapnell, C., Roberts, A., Goff, L., Pertea, G., Kim, D., Kelley, D.R., Pimentel, H., Salzberg, S.L., Rinn, J.L., and Pachter, L. (2012). Differential gene and transcript expression analysis of RNA-seq experiments with TopHat and Cufflinks. Nat. Protoc. 7, 562–578.

Tsai, C.C., Kai, J.I., Huang, W.C., Wang, C.Y., Wang, Y., Chen, C.L., Fang, Y.T., Lin, Y.S., Anderson, R., Chen, S.H., et al. (2009). Glycogen synthase kinase-3beta facilitates IFN-gamma-induced STAT1 activation by regulating Src homology-2 domain-containing phosphatase 2. J Immunol. 183, 856–864.

Van Raemdonck, K., Van den Steen, P.E., Liekens, S., Van Damme, J., and Struyf, S. (2015). CXCR3 ligands in disease and therapy. Cytokine Growth Factor Rev. 26, 311–327.

Wakil, S.J. (1989). Fatty acid synthase, a proficient multifunctional enzyme. Biochemistry 28, 4523–4530.

Wang, K., Yuen, S.T., Xu, J., Lee, S.P., Yan, H.H., Shi, S.T., Siu, H.C., Deng, S., Chu, K.M., Law, S., et al. (2014). Whole-genome sequencing and comprehensive molecular profiling identify new driver mutations in gastric cancer. Nat. Genet. 46, 573–582.

Wang, H., Franco, F., and Ho, P.C. (2017). Metabolic Regulation of Tregs in Cancer: Opportunities for Immunotherapy. Trends Cancer 3, 583–592.

Warburg, O. (1956). On the origin of cancer cells. Science 123, 309–314.

Weber, J.S., D'Angelo, S.P., Minor, D., Hodi, F.S., Gutzmer, R., Neyns, B., Hoeller, C., Khushalani, N.I., Miller, W.H., Jr., Lao, C.D., et al. (2015). Nivolumab versus chemotherapy in patients with advanced melanoma who progressed after anti-CTLA-4 treatment (CheckMate 037): a randomised, controlled, open-label, phase 3 trial. Lancet Oncol. 16, 375–384.

Weinberg, S.E., Singer, B.D., Steinert, E.M., Martinez, C.A., Mehta, M.M., Martínez-Reyes, I., Gao, P., Helmin, K.A., Abdala-Valencia, H., Sena, L.A., et al. (2019). Mitochondrial complex III is essential for suppressive function of regulatory T cells. Nature 565, 495–499.

Wiig, H., Aukland, K., and Tenstad, O. (2003). Isolation of interstitial fluid from rat mammary tumors by a centrifugation method. Am. J. Physiol. Heart Circ. Physiol. 284, H416–H424.

Wing, K., Onishi, Y., Prieto-Martin, P., Yamaguchi, T., Miyara, M., Fehervari, Z., Nomura, T., and Sakaguchi, S. (2008). CTLA-4 control over Foxp3+ regulatory T cell function. Science 322, 271–275.

Yamamoto, M., Nomura, S., Hosoi, A., Nagaoka, K., Iino, T., Yasuda, T., Saito, T., Matsushita, H., Uchida, E., Seto, Y., et al. (2018). Established gastric cancer cell lines transplantable into C57BL/6 mice show fibroblast growth factor receptor 4 promotion of tumor growth. Cancer Sci. 109, 1480–1492.

Yang, C.H., Wei, L., Pfeffer, S.R., Du, Z., Murti, A., Valentine, W.J., Zheng, Y., and Pfeffer, L.M. (2007). Identification of CXCL11 as a STAT3-dependent gene induced by IFN. J Immunol. 178, 986–992.

Yoo, H.Y., Sung, M.K., Lee, S.H., Kim, S., Lee, H., Park, S., Kim, S.C., Lee, B., Rho, K., Lee, J.E., et al. (2014). A recurrent inactivating mutation in RHOA GTPase in angioimmunoblastic T cell lymphoma. Nat. Genet. 46, 371–375.

Zumwalt, T.J., Arnold, M., Goel, A., and Boland, C.R. (2015). Active secretion of CXCL10 and CCL5 from colorectal cancer microenvironments associates with GranzymeB+ CD8+ T-cell infiltration. Oncotarget 6, 2981–2991.